学位申請論文

三浦　伸一

(2)

Thesis:

Theoretical studies on density fluctuations and the stability of an excess electron in liquid water

水の中の密度のゆらぎと過剰電子の安定性に関する理論的研究

Shinichi Miura

Shinichi Miura

Acknowledgments

The author is much grateful to Professor Nobuhiro Go and Professor Fumio Hirata for their extensive support, helpful discussion, and constant encouragement. The author cordially thanks Professor Yosuke Kataoka for his various supports.

The simulation and numerical analysis have been executed in the Computer Center of the Institute for Molecular Science and the workstations of Theoretical Chemistry Laboratory. The author thanks the superusers of workstations in Theoretical Chemistry Laboratory.

Abstract

In this thesis, two problems have been studied. One is the stability of an excess electron in liquid water. This problem has been investigated using integral equation theories, the reference interaction site model (RISM) - polaron theory and the extended RISM theory. A renormalized integral equations based on the closure proposed by Chandler and coworkers is presented. Special attention has been paid to the temperature dependence of the stability of the excess electron. Temperature dependence of the average potential energy and the cavity formation energy of the excess electron has exhibited extrema similar to those observed in various thermodynamic properties of pure water. The correlation between the behavior of the solvation thermodynamic quantities and the structure of liquid water is discussed. The observed red shift of the peak of the optical absorption spectrum with increasing temperature has been successfully reproduced.

The other is collective and single molecule dynamics of mass and charge fluctuation in liquid water. This problem has been investigated theoretically and by the molecular dynamics simulation. Collective modes concerning mass and charge fluctuations have been determined by the projection operator formalism. Amplitudes of each mode in density correlation functions (DCFs) are estimated theoretically. Our theory predicts that at the wavevector $k > 1.0$ Å^{-1} the amplitude of mass mode in charge DCF increases remarkably. This is caused by the coupling of translational mode to the charge fluctuation through the single molecule correlation, which gives slow tail in charge DCF. The dispersion relations of collective modes are discussed. The anomalous acoustic behavior below the wavevector 1.5 Å^{-1} can be well described

by the simple viscoelastic theory. The elastic behavior of charge fluctuation at $k <$ 1.5 $Å^{-1}$ is pointed out.

Table of Contents

A. Static structure factors
B. Eigen frequencies
C. Density correlation functions
D. Optical dynamics
E. Acoustic dynamics
F. Modeling of longitudinal current spectra

IV. Conclusions and problems for future study

I. Introduction

In liquids various fluctuations form and disappear continually. Chemical processes such as solvations and chemical reactions proceed with exciting spatial and temporal fluctuations in liquid environment. The understanding of these processes at molecular level is one of the most important problems in modern chemistry. By the progress of the experimental technique especially in laser spectroscopy, chemical processes in liquid phase have been revealed with the resolution of molecular scale. Solvation of ions and simple chemical reactions in which charged species like electrons and protons are transferred have been studied extensively stimulated by the experimental activity.[1] In this thesis, we addresses two problems. One is the stability of an excess electron in liquid water, which is one of the well-studied systems both theoretically and experimentally. We have investigated this system by the molecular theory of liquid. The other is the collective dynamical behavior of liquid water. This gives the basis to understand the dynamical aspects of chemical processes including the solvation of an excess electron.

An excess electron in liquid water behaves as a distinct chemical species which is well characterized by spectroscopy[2] and exists ubiquitously in irradiated aqueous systems and in electrochemical reactions. This species is called the hydrated electron.[3] In polar liquid, typically in water, an excess electron is spatially localized and its behavior is strongly coupled to the polarization and configuration of the surrounding solvent molecules. The local fluctuations of the solvent, therefore, have to be considered explicitly and the interaction between electron and water molecule

should be treated in non-perturbative fashion. A system consisting of many electrons dissolved in many oxygen and hydrogen atoms gives us a naive description of the hydrated electron. In principle, this problem would be solved by the *ab initio* quantum chemical theory. Unfortunately, the number of molecules to describe liquid state is very large and is beyond the scope of the present day computational method. Consequently, we have to reduce the problem to the tractable model.

For realistic description of the hydrated electron, there are two kinds of reduction. One is a model based on the *ab initio* molecular orbital (MO) theory, that is a negatively charged water cluster embedded in dielectric continuum.[4] In this system called *ab initio* semicontinuum model, a cluster is regarded as a *supermolecule*, hence, its electronic state is solved accurately. However, this kind of model does not include the topological disorder of liquid and does not take the ensemble average in proper way. In particular, this model is not suitable for the hydrogen bonding liquids as water. For instance, Newton carried out the *ab initio* MO calculations of semicontinuum model for the hydrated electron.[4] This calculation predicted that the molecular dipole of water was oriented toward the electron. Kevan and co-workers have carried out the electron spin resonance (ESR) line shape studies of trapped electrons in γ-irradiated alkane glasses to infer the geometrical structure of the localized electron.[5] From such analysis, they concluded that the OH bonds of surrounding water molecules were oriented toward the electron. This result dose not agree with Newton's results based on semicontinuum model. This is due to insufficient number of water molecules included in his calculations to describe detailed hydrogen bond structure among water molecules around the electron. The large number of molecules consisting of cluster would have been needed for

semicontinuum model.

The other model is a model based on the path integral formulation of the quantum mechanics,[6] which is an excess electron dissolved in water interacting with electron-water pseudopotential. With the method, one finds that an electron dissolved in water is isomorphic to a classical polymer dissolved in water.[7] As a result, we can treat the problem of the hydrated electron by means of classical statistical mechanics. According to these ideas, the path integral quantum simulations of the hydrated electron have been carried out by many researchers.[8] From these simulation, many geometrical features of the hydrated electron have been revealed. For example, these simulations have shown that the OH bonds of surrounding water molecules are oriented toward the electron. This is due to the proper treatment of liquid state as opposed to Newton's treatment. Chandler *et al.* developed RISM-polaron theory[9] to treat an excess electron in simple fluid on the basis of the statistical mechanical theory for molecular liquid, reference interaction site model (RISM).[10] This theory has been applied to the excess electron in various liquids.[11]

In chapter II, we have applied the RISM-polaron theory to the problem of the hydrated electron and have investigated the temperature dependence of the stability of the hydrated electron. The questions we have asked are as follows: What determines the stability and its temperature dependence of the excess electron? How do the stability of the electron and the structure of liquid water relate? Particularly, we focused on the relation between the thermodynamic quantities of water and the solvation thermodynamic quantities of the excess electron.

In next chapter, we have investigated the collective dynamical behavior of liquid

water. First, we have to introduce the characteristic modes to be studied. An analogy with the phonon theory of solid state physics leads us at least two characteristic collective modes in polar liquids, i.e., the acoustic mode and the optical mode. These modes correspond respectively to fluctuations in the density of mass and charge.

The acoustic mode in liquid water has been studied as a problem of sound propagation at finite wavelength. Molecular dynamics (MD) simulations have revealed rich dynamical behavior concerning the mode by investigating the center-of-mass density fluctuations.[12,13] In liquid water, a linear dispersion relation has been observed in the wavevector between the range of 0.3 and 1.5 $Å^{-1}$ as in the hydrodynamic regime. However, the associated sound velocity is found to be more than twice higher than the ordinary sound velocity. This behavior was also observed in the experiment of coherent inelastic neutron scattering.[14] This phenomenon leads two controversial explanations. One is that the high sound velocity is associated with a new collective excitation ("fast sound") propagating in the small patches of hydrogen-bonded water molecules.[14] An alternative explanation has been proposed on the basis of the generalized hydrodynamic theory. The high sound velocity is caused by a continuous positive dispersion of the ordinary hydrodynamic sound mode, hence this anomalous behavior can be described by the framework developed for normal liquids.[13,15] This problem is still open to be solved.

The concept of "optical mode" has been introduced to study the dynamical properties of polar liquids. A characteristic mode called dipolar plasmon (or dipolaron) has been obtained by searching the zeros and poles of the dielectric function for the system consisting of Brownian dipoles, which is the dynamical extension of the Onsager theory of the dielectric constant.[16] In this model, the

charge fluctuation is associated with the orientational motion of dipoles. Theoretical formulation to describe the dielectric behavior has been developed with a collective polarization composed of molecular dipoles as the dynamical variable.[17] According to this formalism, the orientational dynamics of molecular dipoles in liquid water has been studied by the MD simulation.[18] Recently, in the MD simulation of liquid water the optic-type excitation has been observed in dynamic structure factor of hydrogen fluctuation.[19] The importance of atomic fluctuation in molecular liquid was stressed in their study. At the wavelength close to intermolecular distance, the detailed molecular structure plays an important role. For polar liquid, the dielectric theory based on the atomic fluctuations has been developed.[20]

In chapter III, the problems we have addressed are as follows. One is the wavevector dependence of the dynamics of charge fluctuation in liquid water. This is important especially for solvation dynamics of ions because the dynamics of charge fluctuation for all wavevector contributes to the solvation process. Attention is paid to the contribution from translational motion of molecules, which plays a significant role to determine the rate of solvation.[1] The other is the anomalous acoustic behavior of liquid water, which is described by the mass fluctuation. A structure which appears at low frequency in the spectrum of the mass current in relatively large wavevectors is interpreted in terms of the single molecule correlation in mass fluctuation. The acoustic dynamics is explained by the simple viscoelastic theory.

Finally, we conclude and present the problems for future study in chapter IV.

References

[1] H. Heitele, Angew. Chem. Int. Ed. Engl. **32**, 359 (1993); B. Bagchi and A. Chandra, Adv. Chem. Phys., **80**, 1 (1991), and references therein.

[2] E. J. Hart and J. W. Boag, J. Phys. Chem. **84**, 4090 (1962).

[3] E. J. Hart and M. Anbar, *The Hydrated Electron* (Wily, New York, 1970).

[4] M. D. Newton, J. Phys Chem. **79**, 2795 (1975).

[5] L. Kevan, J. Phys. Chem. **85**, 1628 (1981).

[6] R. P. Feynman and A. R. Hibbs, *Quantum mechanics and path integrals* (McGraw-Hill, New York, 1965); R. P. Feynman, *Statistical mechanics* (Benjamin, Reading, 1972).

[7] D. Chandler and P. G. Wolynes, J. Chem. Phys. **74**, 4078 (1982).

[8] J. Schnitker, P. J. Rossky, J. Chem. Phys. **86**, 3471 (1987); M. Sprik, R. W. Impey and M. L. Klein, J. Stat. Phys. **43**, 967 (1986); A. Wallqvist, D. Thirumalai, B. J. Berne, J. Chem. Phys. **86**, 6404 (1987); C. D. Jonah, C. Romero, A. Ranman, Chem. Phys. Lett. **123**, 209 (1986).

[9] D. Chandler, Y. Singh, D. M. Richardson, J. Chem. Phys. **81**, 1975 (1984).

[10] D. Chandler, In *The liquid state of matter: fluids, simple and complex*, E. W. Montroll and J. L. Lebowitz, Ed. (North-Holland, Amsterdam, 1982).

[11] A. L. Nichols, D. Chandler, Y. Singh, D. M. Richardson, J. Chem. Phys. **81**, 5109 (1984); D. Laria, D. Chandler, J. Chem. Phys. **87**, 4088 (1987); G. Malescio and M. Parrinello, Phys. Rev. A**35**, 897 (1987); D. Laria, D. Wu, D. Chandler, J. Chem. Phys. **95**, 4444 (1991).

[12] R. W. Impey, P. A. Madden and I. R. McDonald, Mol. Phys. **46**, 513 (1982); F.

Sciortino and S. Sastry, J. Chem. Phys. **100**, 3881 (1994); A. Rahman and F. H. Stillinger, Phys. Rev. A **10**, 368 (1974).

[13] M. Wojcik and E. Clementi, J. Chem. Phys. **85**, 6085 (1986).

[14] J. Teixeira, M. C. Bellissent-Funel, S. H. Chen and B. Dorner, Phys. Rev. Lett. **54**, 2681 (1985).

[15] U. Balucani, G. Ruocco, A. Torcini and R. Vallauri, Phys. Rev. E **47**, 1677 (1993).

[16] R. Lobo, J. E. Robinson and S. Rodriguez, J. Chem. Phys. **59**, 5992 (1973).

[17] P. Madden and D. Kivelson, Adv. Chem. Phys. **56**, 467 (1984), and references therein.

[18] M. Neumann, J. Chem. Phys. **85**, 1567 (1986); D. Bertolini and A. Tani, Mol. Phys. **75**, 1065 (1992).

[19] M. A. Ricci, D. Rocca, G. Ruocco and R. Vallauri, Phys. Rev. A **40**, 7226 (1989).

[20] F. O. Raineri, Y. Zhou, H. L. Friedman and G. Stell, Chem. Phys. **152**, 201 (1991).

II. Stability of excess electron in liquid water

This chapter is organized as follows. In II-1, the theoretical treatment of the solvated electron developed by Chandler and coworkers is briefly outlined. The closure proposed by Laria *et al.*[1] is employed after renormalizing the long ranged interaction. The model studied and the method of calculation are described in II-2. Numerical results and discussions are presented in II-3, where temperature dependence of the behavior of pure water and the hydrated electron is discussed.

II-1. Theoretical basis

A. Outline of theory

We consider the system consisting of an excess electron dissolved in classical molecular solvent. The potential energy of this system can be written as

$$V(\mathbf{r},\{\mathbf{R}_i\}) = V_{es}(\mathbf{r},\{\mathbf{R}_i\}) + V_{ss}(\{\mathbf{R}_i\}) \quad , \tag{1}$$

where

$$V_{es}(\mathbf{r},\{\mathbf{R}_i\}) = \sum_{i=1}^{N} U_{es}(\mathbf{r},\mathbf{R}_i) \quad ,$$

and

$$V_{ss}(\{\mathbf{R}_i\}) = \sum_{i<j}^{N} U_{ss}(\mathbf{R}_i,\mathbf{R}_j) \quad . \tag{2}$$

Here, $\mathbf{r}$ denotes the position of the excess electron, $\mathbf{R}_i$ is the collection of the coordinates for a solvent molecule and N is the number of solvent molecules. In this study, an interaction site model (ISM)[2] is employed as the solvent model. For the ISM molecule, the form of U_{es} and U_{ss} is assumed as

$$U_{es}(\mathbf{r},\mathbf{R}_i)=\sum_{\alpha=1}^{m}u_{e\alpha}\left(\left|\mathbf{r}-\mathbf{r}_i^{\alpha}\right|\right) \quad ,$$

and

$$U_{ss}(\mathbf{R}_i,\mathbf{R}_j)=\sum_{\alpha=1}^{m}\sum_{\gamma=1}^{m}u_{\alpha\gamma}\left(\left|\mathbf{r}_i^{\alpha}-\mathbf{r}_j^{\gamma}\right|\right) \quad , \tag{3}$$

where $\mathbf{r}_i^{\alpha}$ denotes the location of the αth site of the ith solvent molecule and m is the total number of sites of a molecule. Here, $u_{e\alpha}$ is the electron-solvent pseudopotential and $u_{\alpha\gamma}$ is the interaction between solvent molecules. For this system, the canonical partition function in the path integral representation at the inverse temperature β is

$$Z=\int D\mathbf{r}(t)\int d\{\mathbf{R}_i\}\exp\left[-\frac{1}{\hbar}\int_0^{\beta\hbar}dt\left\{\frac{1}{2}m_e|\dot{\mathbf{r}}(t)|^2+V_{es}(\mathbf{r}(t),\{\mathbf{R}_i\})\right\}-\beta V_{ss}(\{\mathbf{R}_i\})\right] \quad , \tag{4}$$

where $\mathbf{r}(t)$ is the electronic path in imaginary time which is periodic in time interval $0 < t < \beta\hbar$ and m_e is the mass of the electron.

To concentrate our attention on the electronic degree of freedom, the partition function given by eq. (4) is rewritten as

$$Z=Z_s\int D\mathbf{r}(t)\exp\{-\beta S_0[\mathbf{r}(t)]-\beta\Delta\mu[\mathbf{r}(t)]\} \quad , \tag{5}$$

with

$$-\beta S_0[\mathbf{r}(t)]=-\frac{1}{\hbar}\int_0^{\beta\hbar}dt\,\frac{1}{2}m|\dot{\mathbf{r}}(t)|^2 \quad ,$$

and

$$\exp\{-\beta\Delta\mu[\mathbf{r}(t)]\}=\left\langle\exp\left\{-\frac{1}{\hbar}\int_0^{\beta\hbar}dtV_{es}(\mathbf{r}(t),\{\mathbf{R}_i\})\right\}\right\rangle_s \quad , \tag{6}$$

where Z_S denotes the partition function of the solvent, $\Delta\mu[\mathbf{r}(t)]$ is the excess chemical potential for the fixed electronic path and $\langle\cdots\rangle_s$ is the configurational average over the solvent degrees of freedom. The quantity $\exp\{-\beta\Delta\mu[\mathbf{r}(t)]\}$ is called the influence functional which represents solvent effects on the quantum degrees of freedom of interest.[3] A functional integral has to be done in eq. (5) to evaluate the excess

chemical potential $\Delta\mu = -\beta^{-1}\ln(Z/Z_s)$ which is an observable quantity in experiment. Here, one can divide this problem into two steps. First, one has to determine the excess chemical potential for the fixed electronic path. Second, one has to evaluate the path integral for the electronic degrees of freedom. According to Chandler's treatment,[4] the first step is carried out by the RISM theory and the second step by the optimized first-order perturbation theory with a reference Gaussian functional, which is called the polaron approximation.

On the basis of the RISM theory, the quantity $\Delta\mu[\mathbf{r}(t)]$ can be represented by

$$-\beta\Delta\mu[\mathbf{r}(t)] = \rho\sum_{\alpha=1}^{n}\hat{c}_{e\alpha}(0) + \frac{1}{2}(\beta\hbar)^{-2}\int_0^{\beta\hbar}dt\int_0^{\beta\hbar}dt' v\left[\left|\mathbf{r}(t)-\mathbf{r}(t')\right|\right] \quad , \tag{7}$$

where ρ denotes the number density of solvent and $\hat{c}_{e\alpha}$ is the spatial Fourier transform of the site-site direct correlation function between the electron and the αth site of the solvent molecule. The function $c_{e\alpha}(r)$ which is defined by the RISM integral equation in the next subsection can be regarded as the interaction between the electron and the solvent site renormalized by the fluctuations in the solvent. The potential of mean force $v(r)$ between two points of the electronic path in imaginary time is written with a mean pair potential approximation,

$$v(r) = -\sum_{\alpha,\gamma=1}^{m} c_{e\alpha} * \chi_{\alpha\gamma} * c_{\gamma e}(r) \quad , \tag{8}$$

where * denotes the convolution integral and $\chi_{\alpha\gamma}$ is the density-density correlation function of the pure solvent defined by $<\delta\rho(\mathbf{r})\delta r(\mathbf{r}')>$.

To complete the evaluation of the excess chemical potential, the electronic path integral still has to be performed. Following Feynman[5] and Chandler *et al.*,[4] the excess chemical potential for the fixed electronic path is mimicked by a Gaussian functional,

$$-\beta\Delta\mu_{ref}[\mathbf{r}(t)] = r_0 + \frac{1}{2}(\beta\hbar)^{-2}\int_0^{\beta\hbar} dt \int_0^{\beta\hbar} dt' \Gamma(t-t')|\mathbf{r}(t)-\mathbf{r}(t')|^2 \quad , \tag{9}$$

where $\Gamma(t\text{-}t')$ is a solvent-induced force constant between two points of the electronic path in imaginary time and r_0 gives the zero of the energy. The Gibbs-Bogoliubov-Feynman inequality[3,6] provides an upper bound for the excess chemical potential,

$$\Delta\mu \le -\beta^{-1}\ln Z_{ref} + \left\langle \Delta\mu[\mathbf{r}(t)] - \Delta\mu_{ref}[\mathbf{r}(t)] \right\rangle_{ref} \quad . \tag{10}$$

Here, Z_{ref} is the electronic partition function for the Gaussian reference system and $\langle\cdots\rangle_{ref}$ means the average over the reference system weight determined by $S_0[\mathbf{r}(t)] + \Delta\mu_{ref}[\mathbf{r}(t)]$. Minimizing the right-hand side of eq. (10) provides the optimal Gaussian reference system. This procedure gives a set of equations as follows. The spatial Fourier transform of the equilibrium response function for the electron is

$$\begin{aligned} \omega(k,\tau) &= \left\langle \exp\left\{ i\mathbf{k}\cdot[\mathbf{r}(\tau)-\mathbf{r}(0)] \right\} \right\rangle_{ref} \\ &= \exp\left[-k^2 R^2(\tau)/6\right] \quad , \end{aligned} \tag{11}$$

where $R^2(\tau)$ is the mean square correlation function in imaginary time given by

$$R^2(\tau) = \left\langle |\mathbf{r}(t)-\mathbf{r}(t')|^2 \right\rangle = 6\sum_n \frac{1}{\beta m \Omega_n^{\,2} + \gamma_n}[1-\cos\Omega_n\tau] \quad . \tag{12}$$

Here, $\tau = t\text{-}t'$, $\Omega_n = 2\pi n/\beta\hbar$ and γ_n is the friction constant written by

$$\gamma_n = -\frac{1}{6\pi^2\beta\hbar}\int_0^{\infty} dk \int_0^{\beta\hbar} d\tau \hat{v}(k) k^4 [1-\cos\Omega_n\tau]\omega(k,\tau) \quad . \tag{13}$$

Owing to a Gaussian reference functional, the electron response function is completely determined by the second moment $R^2(\tau)$. For a free electron, the second moment is given analytically by[7]

$$R_{free}^{\,2}(\tau) = 3\lambda_e^{\,2}\tau(\beta\hbar-\tau)/(\beta\hbar)^2 \quad , \tag{14}$$

where $\lambda_e^{\,2} = \beta\hbar^2/m_e$. Equations (11), (12), and (13) construct the polaron approximation.

B. The renormalized integral equation

To calculate the excess chemical potential for the fixed electronic path, the site-site direct correlation function between the electron and the solvent site have to be determined. This is carried out by means of the RISM equation written with a mean field approximation,[4]

$$h_{e\alpha}(r) = \sum_{\gamma=1}^{m} \left\{ \omega_e * c_{e\gamma} * \omega_{\gamma\alpha}(r) + \omega_e * c_{e\gamma} * \rho h_{\gamma\alpha}(r) \right\} \quad , \tag{15}$$

with

$$\omega_e(|\mathbf{r}-\mathbf{r}'|) = \frac{1}{\beta\hbar} \int_0^{\beta\hbar} d\tau \omega(|\mathbf{r}-\mathbf{r}'|;\tau) \quad , \tag{16}$$

where $\omega_{\alpha\gamma}(r)$ is the intramolecular correlation function of the solvent molecule, $h_{e\alpha}$ and $h_{\alpha\gamma}$ are the pair correlation function between the electron and the solvent sites and between a pair of solvent sites, respectively.

The HNC-like closure was used in spirit of the extended RISM theory[8,9] for an electron in the molten salts.[10] In the case of the hydrated electron, however, the converged solution cannot be obtained by the HNC-like closure.[1] We employed the closure relation proposed by Laria *et al.* which is derived by an optimized perturbation theory:

$$\ln[1 + h_{e\alpha}(r)] = -\beta \bar{u}_{e\alpha}(r) - \beta \Delta w_{e\alpha}(r) \quad , \tag{17}$$

with

$$-\beta \Delta w_{e\alpha}(r) = \sum_{\gamma=1}^{m} \omega_e * c_{e\gamma} * \rho h_{\gamma\alpha}(r) \quad , \tag{18}$$

where the function with a bar, $\bar{X}_{e\alpha}$ is defined by $\bar{X}_{e\alpha} = \sum_{\gamma=1}^{m} \omega_e * X_{e\gamma} * \omega_{\gamma\alpha}(r)$. For an atomic solvent, this closure reduces to the HNC-like closure. Owing to the long ranged part in the interactions between the electron and the solvent molecule, the renormalized form of the integral equation is desired. To derive the renormalized

integral equation, the interaction divides into two parts: a short ranged part $\phi_{e\alpha}^{*}$ and a long ranged part $\phi_{e\alpha}$ such that

$$-\beta u_{e\alpha}(r) = \phi_{e\alpha}^{*}(r) + \phi_{e\alpha}(r) \quad . \tag{19}$$

We assume here that the asymptotic form of the direct correlation function is given by $c_{e\alpha}(r) \to \phi_{e\alpha}(r)$ for large r. Using the function $\phi_{e\alpha}(r)$, the short-ranged direct correlation function can be defined by

$$c_{e\alpha}^{s}(r) = c_{e\alpha}(r) - \phi_{e\alpha}(r) \quad . \tag{20}$$

With the help of $c_{e\alpha}^{s}$, we can rewrite eq. (15) as

$$h_{e\alpha}(r) = \gamma_{e\alpha}(r) + \sum_{\gamma=1}^{m} \omega_{e} * c_{e\gamma}^{s} * \left\{ \omega_{\gamma\alpha}(r) + \rho h_{\gamma\alpha}(r) \right\} \quad , \tag{21}$$

with

$$\gamma_{e\alpha}(r) = \sum_{\gamma=1}^{m} \omega_{e} * \phi_{e\gamma} * \left\{ \omega_{\gamma\alpha}(r) + \rho h_{\gamma\alpha}(r) \right\} \quad . \tag{22}$$

A second auxiliary function is introduced as

$$\theta_{e\alpha}(r) = \sum_{\gamma=1}^{m} \omega_{e} * c_{e\gamma}^{s} * \left\{ \omega_{\gamma\alpha}(r) + \rho h_{\gamma\alpha}(r) \right\} - \bar{c}_{e\alpha}^{s}(r) \quad . \tag{23}$$

As a result, eq. (21) becomes

$$h_{e\alpha}(r) = \bar{c}_{e\alpha}^{s}(r) + \theta_{e\alpha}(r) + \gamma_{e\alpha}(r) \quad . \tag{24}$$

Using these functions, the closure relation eq. (17) can be written as

$$\bar{c}_{e\alpha}^{s}(r) = \exp\left[\phi_{e\alpha}^{*}(r) + \theta_{e\alpha}(r) + \gamma_{e\alpha}(r) \right] - \theta_{e\alpha}(r) - \gamma_{e\alpha}(r) - 1 \quad . \tag{25}$$

In the end, eqs. (24) and (25) are the final form of the renormalized integral equation.

II-2. Computational Details

A. Models

Several groups have performed the quantum simulation of the hydrated electron.[11-14] Sprik *et al.*[13] employed the SPC model[15] as a solvent model and the electron-water pseudopotential given by

$$\begin{aligned} u_{e\alpha}(r) &= -ez_\alpha/R_\alpha, \quad r < R_\alpha \quad , \\ &= -ez_\alpha/r, \quad r \geq R_\alpha \quad , \end{aligned} \tag{26}$$

where z_α is a partial charge on the α site of the SPC model and R_α is the cutoff distance. R_α is zero for the oxygen site and 1 Å for the hydrogen site. In our calculations, the modified SPC model was used, which has a small core at the hydrogen site to avoid numerical difficulty. For the electron-water pseudopotential, the functional form of eq. (26) was employed with a slightly different choice from Sprik *et al.*, R_α = 0.92 Å, for the hydrogen site. As pointed out by Laria *et al.* the electronic state causes a transition as the cutoff distance R_H is increased. In our calculation, the transition occurred between 0.92 and 0.93 Å, which is slightly different from that found by Laria *et al.*, 0.95 Å < R_H < 0.97 Å. This difference is due to using the different structure factor for water. While they obtained the structure factor from the MD simulation of pure water, we calculated from the extended RISM theory with HNC-like closure modified to reproduce the correct long-range behavior of the site-site pair correlation functions.[16] The experimental dielectric constants which are needed for the correction are obtained from the reference.[17] To study the temperature dependence at a constant pressure of 1 atm, thermodynamic parameters are taken from the reference.[17]

B. Methods of calculations

The computational procedure for RISM-polaron calculations is organized as follows. The n-th estimate for the equilibrium response function of the electron $\omega^{(n)}$

is first given. Using $\omega^{(n)}$, the n-th estimate of the pair correlation functions and the direct correlation functions are calculated via the RISM equation (24) and (25). From eq. (11), the $(n+1)$-th estimate of ω can be obtained with the aid of the n-th estimate of the direct correlation functions. We continue this loop until the self-consistency condition is satisfied. The initial estimate for ω is the free electron correlation function given by eq. (14).

To solve the RISM equation (24) and (25) numerically, we used the standard iterative method, the Picard procedure, with a mixing ratio p defined as

$$\theta_{e\alpha}^{(n+1)}(r) = p\theta_{e\alpha}^{(n)}(r) + (1-p)\theta_{e\alpha}^{(n-1)}(r) \quad . \tag{27}$$

The Fourier transforms were performed with the Talman algorithm[18] which was implemented for the spherically symmetric transforms by Rossky and Friedman on a logarithmically spaced grid.[19] We used 512 grid points in all calculations of this work. To check the convergence of the calculations, we introduced the root mean square difference of the θ functions in two successive iterations defined by

$$\Delta_{e\alpha} = \left[\sum_{i=1}^{M} \left\{ \theta_{e\alpha}^{(n+1)}(r_i) - \theta_{e\alpha}^{(n)}(r_i) \right\}^2 / M \right]^{1/2} \quad , \tag{28}$$

where i was spatial grid number and M was the total number of spatial grid points. The convergence criterion $\Delta_{e\alpha} < 10^{-6}$ was used.

To calculate eq. (12), we have to evaluate the infinite summation. The approximate $R^2(\tau)$ was given by[10]

$$R^2(\tau) \approx \sum_{n \le \bar{n}} \frac{1}{\beta m \Omega_n^{\,2} + \gamma_n} \left[1 - \cos(\Omega_n \tau) \right] + \sum_{n > \bar{n}} \frac{1}{\beta m \Omega_n^{\,2}} \left[1 - \cos(\Omega_n \tau) \right] \quad . \tag{29}$$

The infinite summation of eq. (29) was evaluated from

$$\sum_{n > \bar{n}} \frac{1}{\beta m \Omega_n^{\,2}} \left[1 - \cos(\Omega_n \tau) \right] = R_{free}^{\,2}(\tau) - \sum_{n \le \bar{n}} \frac{1}{\beta m \Omega_n^{\,2}} \left[1 - \cos(\Omega_n \tau) \right] \quad . \tag{30}$$

We have found that $\bar{n}$ = 100 gives $R^2(\tau)$ which is accurate enough to approximate

the summation. With these functions the next estimate of ω can be calculated. The convergence criterion for ω, that is the root mean square difference of two successive estimate, is less than 10^{-6}.

II-3. Results and discussion

A. Spatial density correlations of water

We first show the site-site radial distribution functions (RDFs) to discuss the structure of water and its temperature effects. These functions are needed for the RISM-polaron calculations to construct the density-density correlation function. The structure of liquid water is closely related to the stability of the hydrated electron. In Fig. 1, the site-site RDFs of the O-H pairs of water are depicted. The first peak indicates the hydrogen bonding between water molecules. The height of this peak was reduced as temperature increases. This behavior implies that hydrogen bonding between water molecules is broken or distorted.

It is well-known that the temperature dependence of the thermodynamic quantities of water shows many anomalous behaviors.[17] Isothermal compressibility χ_T gives one example, which has a minimum around 45 °C as temperature increases. The isothermal compressibility is related to the zero wavevector component of the density-density correlation functions between any two sites by[2]

$$\chi_T = \frac{1}{\rho^2 k_B T} \hat{\chi}_{\alpha\gamma}(0) \quad . \tag{31}$$

Fig. 2 shows the results obtained from the extended RISM theory. One can observe that the χ_T has a minimum with increasing temperature. This behavior agrees with the experiment qualitatively. Theoretical results overestimate the magnitude of χ_T

and give a higher temperature for the minimum. Nevertheless, to our knowledge this is the first study to reproduce the minimum of χ_T for liquid water from the first principle. What is the origin for the minimum of χ_T? For normal liquids, the isothermal compressibility grows monotonously with increasing temperature. It is due to an increase in the average molecular distance, which is, in turn, caused by the anharmonicity of the potential surface. The increased distance to be compressed by applied pressure gives rise to the greater compressibility. In the case of liquid water, there is an opposing factor which is caused by disruption of the hydrogen bond with increasing temperature. The disruption of the hydrogen bond causes local close packing which gives rise to the low compressibility. These competing factors make a minimum at a certain temperature.

B. Imaginary time response of the electron and the electron-water radial distribution functions

The equilibrium response of the electron can be described by the correlation function $\omega(k,\tau)$. This function is completely determined by the mean square displacement of the electron in imaginary time, $R^2(\tau)$ due to the Gaussian approximation (9). Fig. 3 shows the converged results for $R(\tau)$ at 25 °C. The free electron correlation function is also shown for comparison. We can see the localization of the excess electron in liquid water. Theoretical result is in good agreement with the simulation except underestimating the size of the electronic distribution. The characteristic size of the electronic distribution is described by $R(\beta\hbar/2)$ which is called a correlation length. From the theoretical result, the correlation length is $R(\beta\hbar/2) \approx 2.9$ Å which was comparable with the diameter of a

water molecule. In Fig. 4, the RDFs between the electron and water molecules at 25 °C are exhibited. Theoretical results were qualitatively in good agreement with the simulation and reproduce the weak radial correlations between the electron and water molecules. However, the surrounding water molecules are kept at a slightly further distance from the electron than what is observed in the simulation. This is a reason why the size of the electronic distribution is underestimated. These results are in good agreement with those of Laria *et al.* Here, note that there is the population of the excess electron around the hydrogen in water molecules as seen in the electron-hydrogen RDF. This implies that the excess electron soaks into the water molecules. We will see later this overlap of hydrogen atoms and the electron causes an anomalous behavior for the temperature dependence of the electron-water interaction energy.

C. Stability of the hydrated electron and its temperature dependence

To discuss the stability of the excess electron, we evaluate the excess chemical potential given by[1]

$$\beta\Delta\mu = -\rho\sum_{\alpha}\hat{c}_{e\alpha}(0) - 3\sum_{n\geq 1}\left[\frac{\gamma_n}{\beta m\Omega_n^{\,2}+\gamma_n} - \ln\left(1+\frac{\gamma_n}{\beta m\Omega_n^{\,2}}\right)\right] + \frac{1}{4\pi^2}\int_0^\infty dk\,k^2\hat{v}(k)\hat{\omega}(k) \quad . \qquad (32)$$

The experimental value of $\Delta\mu$ has been estimated by a thermodynamic cycle analysis of the electrochemical measurements.[20] At 25 °C, the value of $\Delta\mu$ is -1.62 eV from the experiment and -0.96 eV from our result. Fig. 5 shows the temperature dependence of $\Delta\mu$ obtained from the RISM-polaron calculations. As the temperature increases, the excess chemical potential decreases, that is, the excess electron stabilizes. What stabilizes the excess electronic state? To make the temperature dependence clear we decompose the excess chemical potential into its constituent elements. The internal

energy to the chemical potential can be split into three contributions: the average kinetic energy <*ke*>, the average potential energy <*pe*>, and the solvent reorganization energy. Yu and Karplus have proven that the reorganization energy and its entropy counterpart exactly cancel each other.[21] Consequently the chemical potential consists of three contributions: <*ke*>, <*pe*> and the rest of the entropy contribution associated with the work to make the fluctuating cavity. In this paper, we call the last contribution the cavity formation energy <*cfe*>. The calculated value for each contribution is <*ke*> = 1.82 eV, <*pe*> = -6.08 eV and <*cfe*> = 3.30 eV at 25 °C, respectively. The three contributions cancel each other, so that $|\Delta\mu|$ is small. The sign of $\Delta\mu$ is determined by the average potential energy.

In Fig. 6 (a), we show the temperature dependence of the average kinetic energy of the excess electron. The kinetic energy enhances as the cavity size in which the electron is confined becomes less. For RISM-polaron theory, the average kinetic energy of the excess electron can be written by[10]

$$\langle ke \rangle = \frac{3}{2} k_B T \left(1 + \sum_{n \neq 0} \frac{\gamma_n}{\beta m \Omega_n^{\,2} + \gamma_n} \right) \quad . \tag{33}$$

Here, the first term in eq. (33) is the average kinetic energy of the free electron and the second term is the excess kinetic energy due to the electron confinement in a small cavity. For the hydrated electron, the latter term is dominant and the contribution from the former is only 2% at 25 °C. The average kinetic energy diminished with rising temperature. This is because the void space where the electron localizes expands due to the reduction of the density of water as temperature increases.

Fig. 6 (b) depicts the average potential energy of the electron defined by

$$\langle pe \rangle = \rho \sum_{\alpha} \int dr g_{e\alpha}(r) u_{e\alpha}(r) \quad . \tag{34}$$

The temperature dependence of the average potential energy shows unexpected behavior. The average potential energy gives a minimum value around 40 °C. As the hydrogen bond between the water molecules is disrupted with rising temperature, the rotational motion of water molecules enhances. The increase in rotational motion gives rise to two effects in terms of the electron-water interaction. The first effect makes the effective charge distribution of the water molecules spherically more symmetrical, which in turn makes the electrostatic potential energy between the water molecules and the electron more positive. The second effect causes an enhanced overlap between the water hydrogen and electron, which makes the electrostatic potential energy more negative. The two effects counterbalance each other to give a minimum at a temperature. At lower temperature, the latter effect dominates. For supporting this statement we show the value of the electron-hydrogen RDF around r = 0 Å, $g_{eH}(0)$ in Fig. 7. This value represents a degree of overlap between the electron and hydrogen atom, and hence is closely related to the potential energy between them. As the temperature increases, the value of $g_{eH}(0)$ increases. Under 40 °C this value grows more rapidly than that at higher temperature. This gives indirect evidence for our speculation.

In Fig. 8, we show the cavity formation energy defined by $\langle cfe \rangle = \Delta\mu - \{\langle ke \rangle + \langle pe \rangle\}$. This quantity has a maximum with increasing temperature. As we see above, the isothermal compressibility of water decreases at low temperature and increases at high temperature. This implies that the energy to make the cavity increases at low temperature and decreases at high temperature. This can be the origin of the maximum of the cavity formation energy.

Shown in Fig. 9 is the *classical* excess chemical potential defined by subtracting

the kinetic energy from the excess chemical potential. It is interesting that its temperature dependence is contrary to the *quantum* excess chemical potential. For comparison, the excess chemical potential for Cl^-, which is calculated by the extended RISM theory, is also shown in Fig. 9. The excess chemical potential increases as the temperature increases. This is the same temperature dependence as the *classical* excess chemical potential of the hydrated electron. Furthermore, in the case of the hydrated electron, this monotonous dependence on temperature is a result of canceling the average potential energy and the cavity formation energy which have the opposite temperature dependence. From these results, it is concluded that the temperature dependence of $\Delta\mu$ is essentially determined by that of the kinetic energy.

The anomalous behavior in the thermodynamic quantities predicted above can be in principle verified by experiments. We suggest, in what follows, an experiment which may be possible. First we define a quantity to which we refer to as the binding energy which is the sum of the average kinetic energy and the average potential energy. The binding energy is the energy required to detach an electron from the liquid water without allowing nuclear rearrangement to occur. This quantity can be measured in photoelectron spectroscopy for an excess electron in a cluster.[22] Unfortunately, such a measurement has not been reported for the hydrated electron in liquid. In Fig. 10, the binding energy of the electron are depicted. The binding energy gives a minimum value around 60 °C as the temperature increases. This quantity gives us a test to check our results, if we can measure it for the hydrated electron.

D. Electronic excitation energy

The first electronic excitation energy can be estimated from $R^2(\tau)$. When there is ground state dominance which is a characteristic of the localized state, the function $R^2(\tau)$ starts from zero at τ = 0 and rapidly reaches a plateau value. The characteristic rise time τ_c of this initial imaginary time dependence is a measure of the energy difference ΔE between the ground state and the first manifold of excited states. ΔE may be obtained as[7]

$$\Delta E = \frac{\hbar}{\tau_c} \quad . \tag{35}$$

We employ linear regression applied to the logarithm of $R^2(\beta\hbar/2) - R^2(\tau)$ to estimate ΔE. It is expedient to employ the imaginary time interval between 0 and $0.02\beta\hbar$. These data are very accurately fitted. The values of ΔE are 1.73 eV from experiment,[23] 2.1 eV from simulation, and 2.6 eV from our calculation. Our calculation overestimates the absolute value of ΔE compared to the experiment and the simulation. On the other hand, the temperature dependence of ΔE, which is shown in Fig. 11, is very good agreement with the experiment. Our calculated results give $d\Delta E/dT$ = -0.0035 eV/°C and the experimental result $d\Delta E/dT$ = -0.003 eV/°C.[24] Here we comment on the reliability of ΔE estimated from rise time. The excitation energy has a distribution due to the topological disorder of the solvent. In the case of the hydrated electron, the absorption spectrum was calculated by Schnitker *et al.* using a pseudopotential which was very close numerically to that employed by us. The absorption spectrum gave a maximum at 2.4 eV, which agreed closely with the value estimated from the rise time, 2.2 eV. The agreement between the two methods of estimating the peak position of the absorption spectrum gives us partial confidence concerning the reliability of ΔE estimated from the rise time. It

should be pointed out that this gives only a rough estimate of the excitation energy. For a more accurate evaluation real time methods are necessary.[25,26]

References

[1] D. Laria, D. Wu and D. Chandler, J. Chem. Phys. **95**, 4444 (1991).

[2] J. P. Hansen and I. R. McDonald, *Theory of simple liquids* (Second Edition, Academic Press, 1986).

[3] R. P. Feynman and A. R. Hibbs, *Quantum mechanics and path integrals* (McGraw-Hill, New York, 1965).

[4] D. Chandler, Y. Singh and D. M. Richardson, J. Chem. Phys. **81**, 1975 (1984).

[5] R. P. Feynman, Phys. Rev. **97**, 660 (1955).

[6] R. P. Feynman, *Statistical mechanics* (Addison-Wesley, 1972).

[7] A. L. Nichols, D. Chandler, Y. Singh and D. M. Richardson, J. Chem. Phys. **81**, 5109 (1984).

[8] F. Hirata, B. M. Pettitt and P. J. Rossky, J. Chem. Phys. **77**, 509 (1982).

[9] F. Hirata, P. J. Rossky and B. M. Pettitt, J. Chem. Phys.**78**, 4133 (1983).

[10] G. Malescio and M. Parrinello, Phys. Rev. **A35**, 897 (1987).

[11] C. D. Jonah, C. Romero and A. Ranman, Chem. Phys. Lett. **123**, 209 (1986).

[12] J. Schnitker and P. J. Rossky, J. Chem. Phys. **86**, 3471 (1987).

[13] M. Sprik, R. W. Impey and M. L. Klein, J. Stat. Phys. **1986**, 976 (1986).

[14] A. Wallqvist, D. Thirumalai and B. J. Berne, J. Chem. Phys. **86**, 6404 (1987).

[15] H. J. C. Berendsen, J. P. M. Postma, W. F. V. Gunsteren and J. Hermans, In *Intermolecular Forces*, edited by B. Pullman (Reidel, Dordrecht, 1981), p 331.

[16] P. T. Cummings and G. Stell, Mol. Phys. **46**, 383 (1982).

[17] D. Eisenberg and W. Kauzmann, *The structure and properties of water* (Oxford, London, 1969).

[18] J. D. Talman, J. Comp. Phys. **29**, 35 (1978).

[19] P. J. Rossky and H. L. Friedman, J. Chem. Phys. **72**, 5694 (1980).

[20] J. Jortner and R. M. Noyes, J. Phys. Chem. **70**, 770 (1966).

[21] H. Yu and M. Karplus, J. Chem. Phys. **89**, 2366 (1988).

[22] J. C. Coe, G. H. Lee, J. G. Eaton, S. T. Arnold, H. W. Sarkas, K. H. Bowen, C. Ludewigt, H. Haberland and D. R. Worsnop, J. Chem. Phys. **92**, 3980 (1990).

[23] E. J. Hart and M. Anbar, *The Hydrated Electron* (Wily, New York, 1970).

[24] B. D. Michael, E. J. Hart and K. H. Schmidt, J. Phys. Chem. **75**, 2798 (1971).

[25] B. J. Berne and D. Thirumalai, Ann. Rev. Phys. Chem. **37**, 401 (1986).

[26] J. D. Doll, D. L. Freeman and T. L. Beck, Adv. Chem. Phys. **78**, 61 (1990).

Figure captions

Fig. 1: The O-H radial distribution function for water at constant pressure, 1 atm. Solid line, T = 25 °C: dashed line, T = 50 °C: dot-dashed line, T = 90 °C.

Fig. 2: Isothermal compressibility of liquid water. The solid line is obtained from the extended RISM theory. The circles are experimental values taken from reference.

Fig. 3: Root mean square correlation function $R(\tau)$ of the hydrated electron. Solid line, free electron: dashed line, theoretical result: circle, simulation result.

Fig. 4:Electron-water radial distribution functions. The solid lines are the theoretical results for the electron-hydrogen pair and for the electron-oxygen pair. The circles are the simulation results.

Fig. 5: Temperature dependence of the excess chemical potential of the electron.

Fig. 6: Temperature dependence of the average kinetic energy (a, top) and the average potential energy of the electron (b, bottom).

Fig. 7: Value of the electron-hydrogen radial distribution function at r = 0 Å, $g_{eH}(0)$.

Fig. 8: Cavity formation energy of the electron defined by $\langle cfe \rangle = \Delta\mu - \{\langle ke \rangle + \langle pe \rangle\}$.

Fig. 9: Classical excess chemical potential of the electron (solid line) defined by $\Delta\mu_{cl}$ = $\Delta\mu$ - $\langle ke \rangle$. The dashed line is for the excess chemical potential of Cl^-.

Fig. 10: Binding energy of the electron defined by a sum of the average kinetic energy and the average potential energy.

Fig. 11: First excitation energy of the electron. The circle is the theoretical value estimated from $R^2(\tau)$. The solid line is obtained by least square fitting to the theoretical values. The dashed line is obtained from experiment.

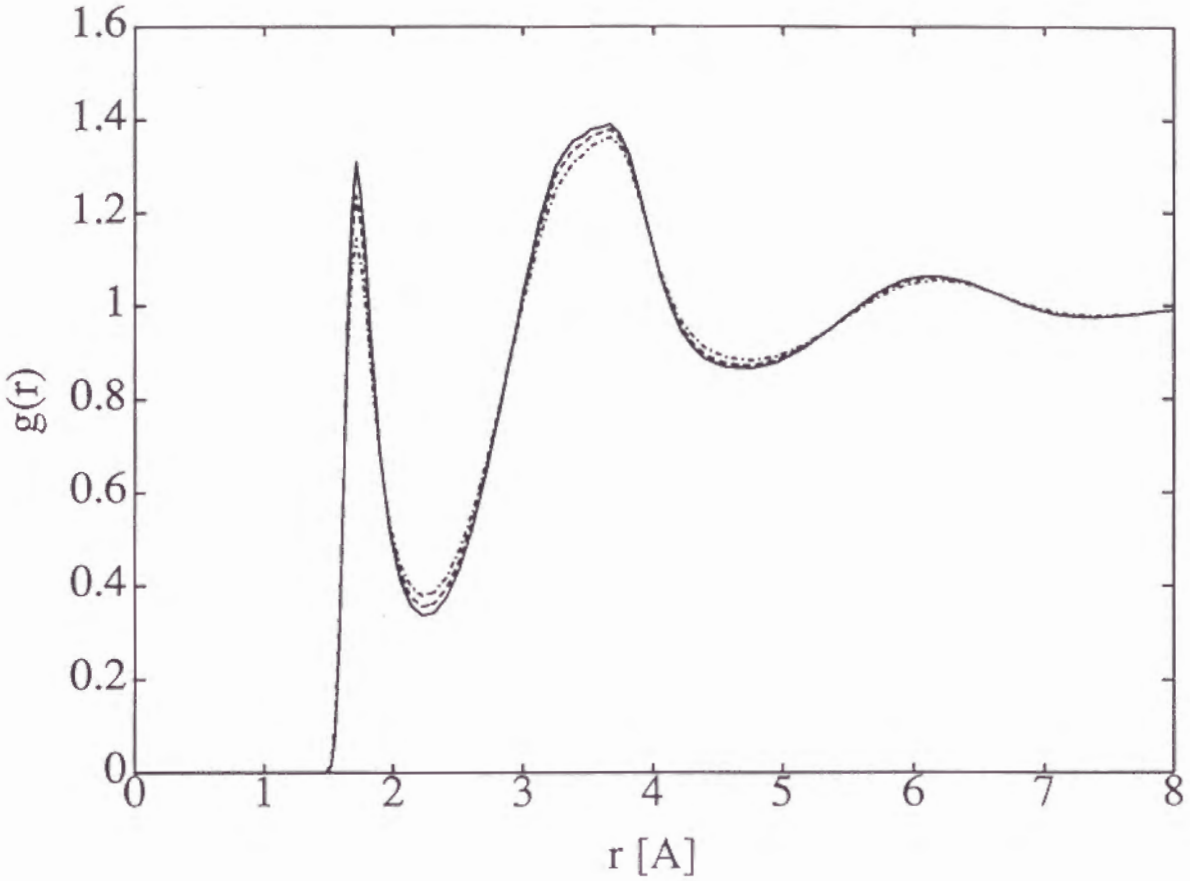

Fig. 1

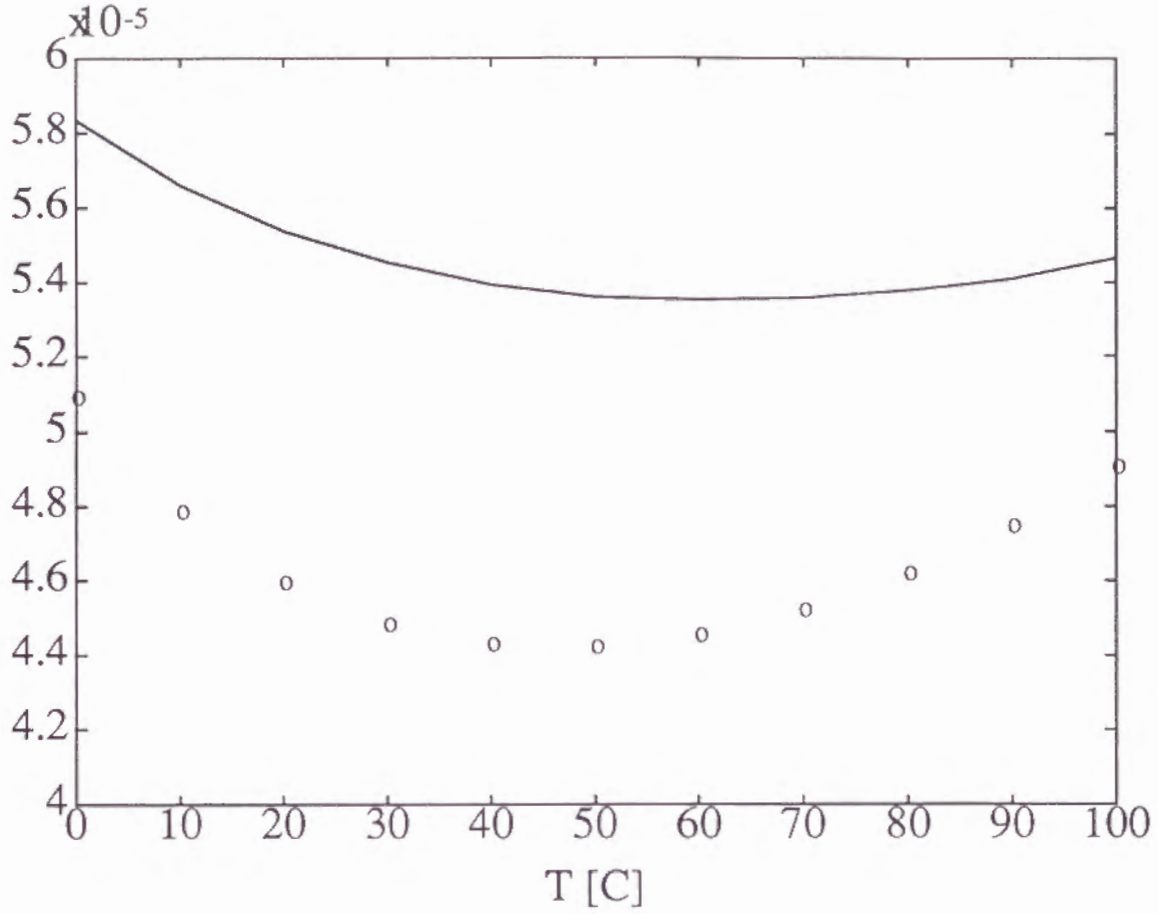

Fig. 2

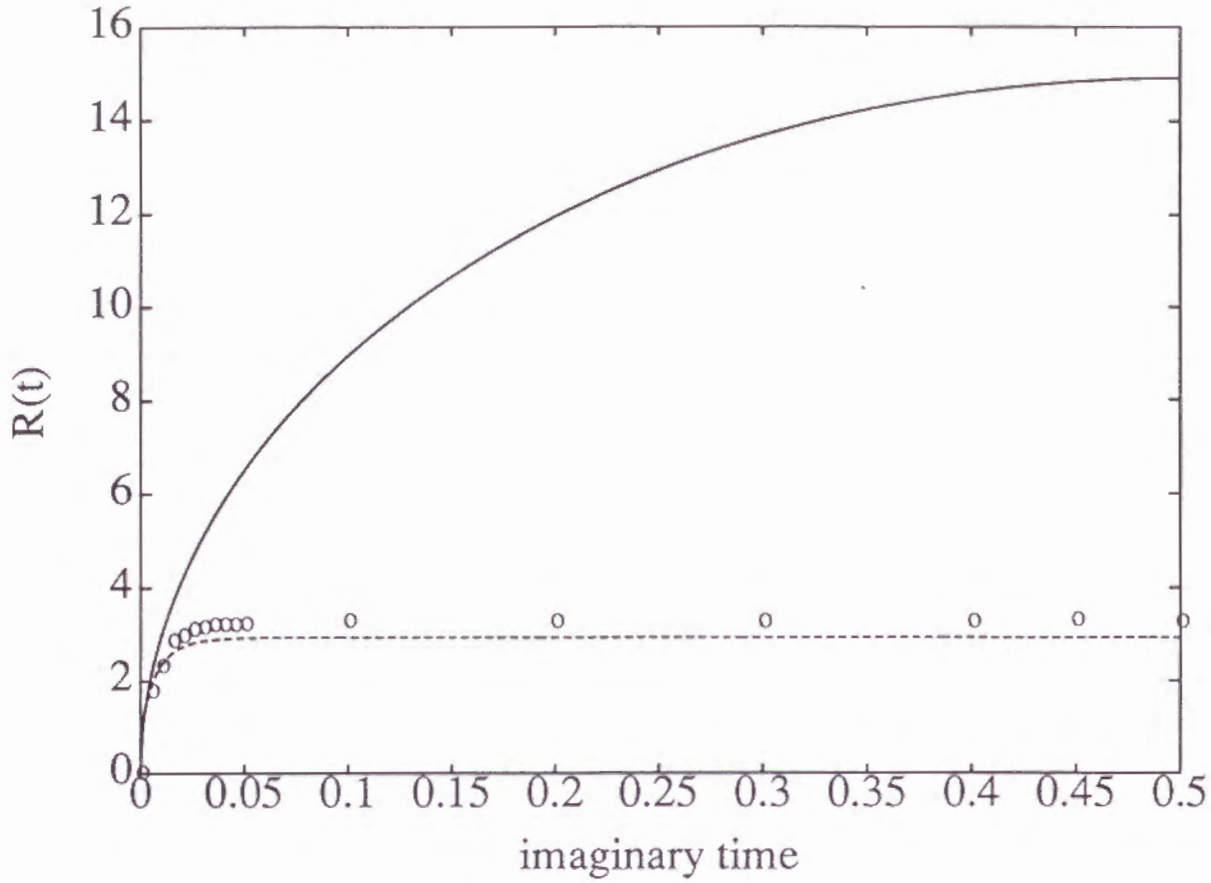
16
14
12
10
8
6
4
2
0
R(t)
0
0.05
0.1
0.15
0.2
0.25
0.3
0.35
0.4
0.45
0.5
imaginary time

Fig. 3

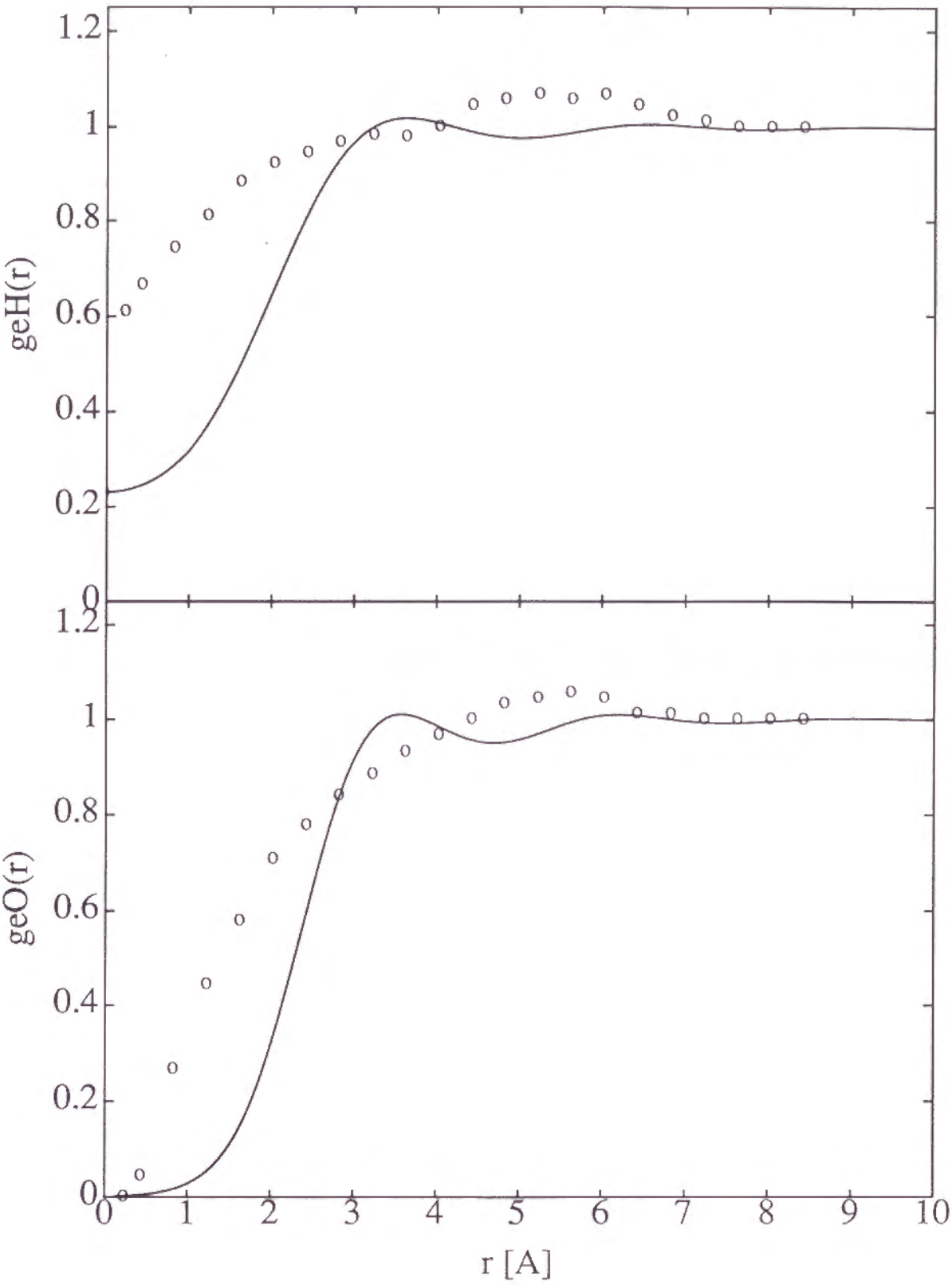

Fig. 4

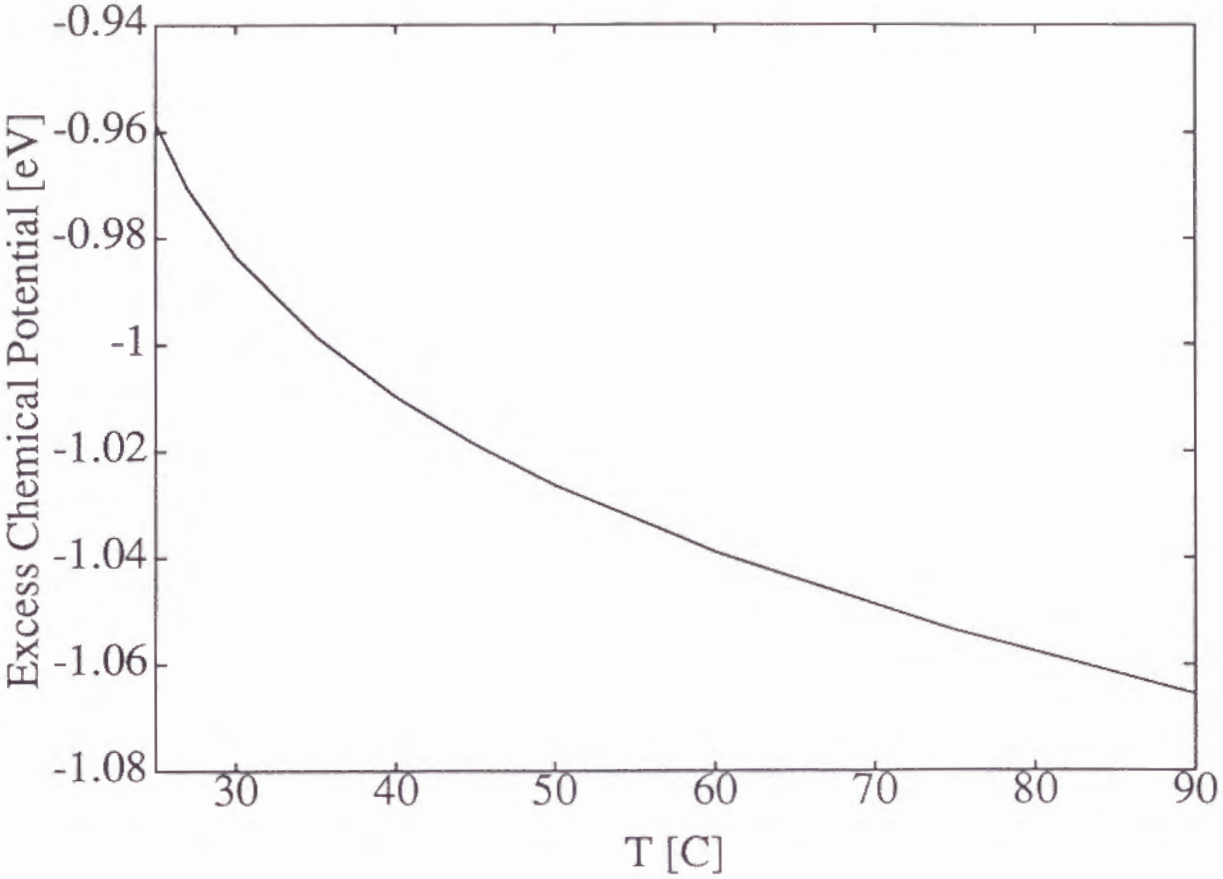
-0.94
-0.96
-0.98
-1
-1.02
-1.04
-1.06
-1.08
Excess Chemical Potential [eV]
30
40
50
60
70
80
90
T [C]

Fig. 5

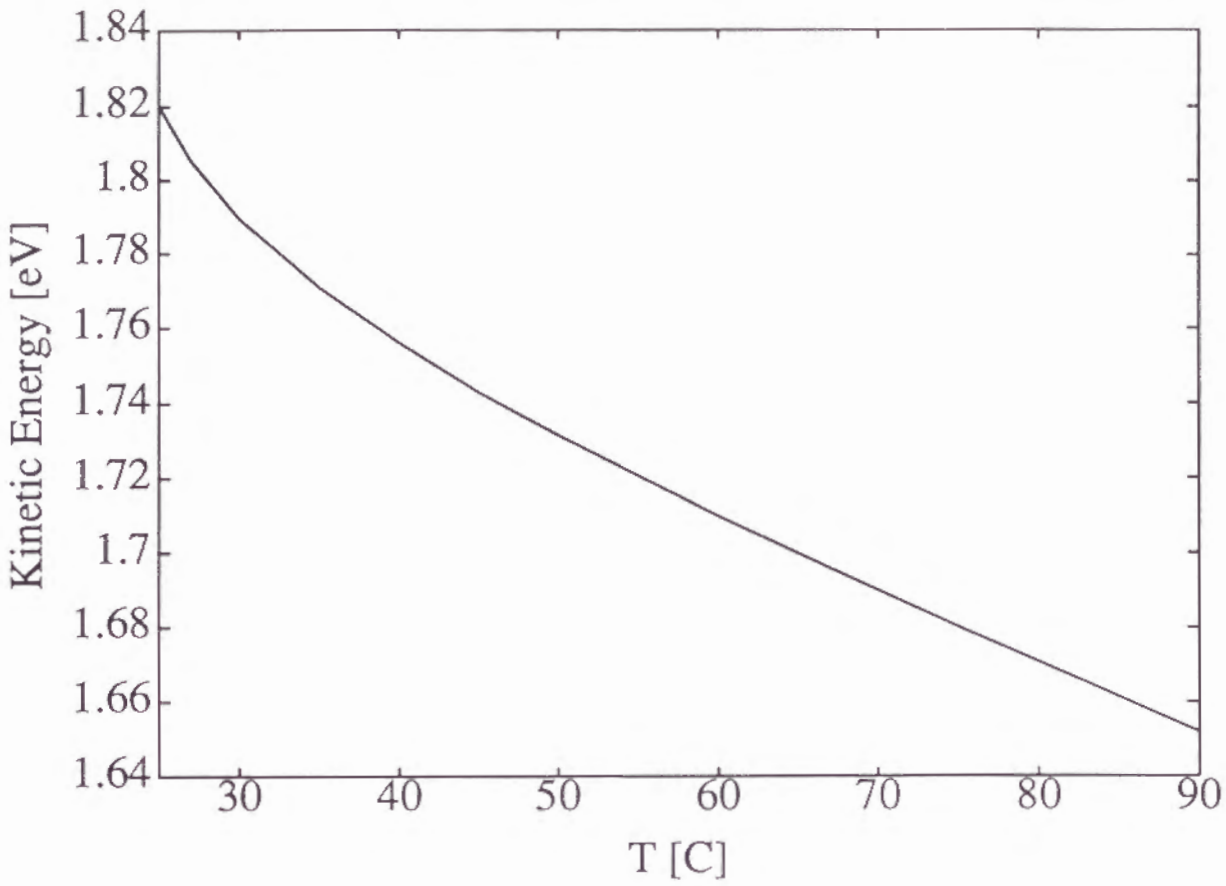
Kinetic Energy [eV]
1.84
1.82
1.8
1.78
1.76
1.74
1.72
1.7
1.68
1.66
1.64
30
40
50
60
70
80
90
T [C]

Fig. 6 (a)

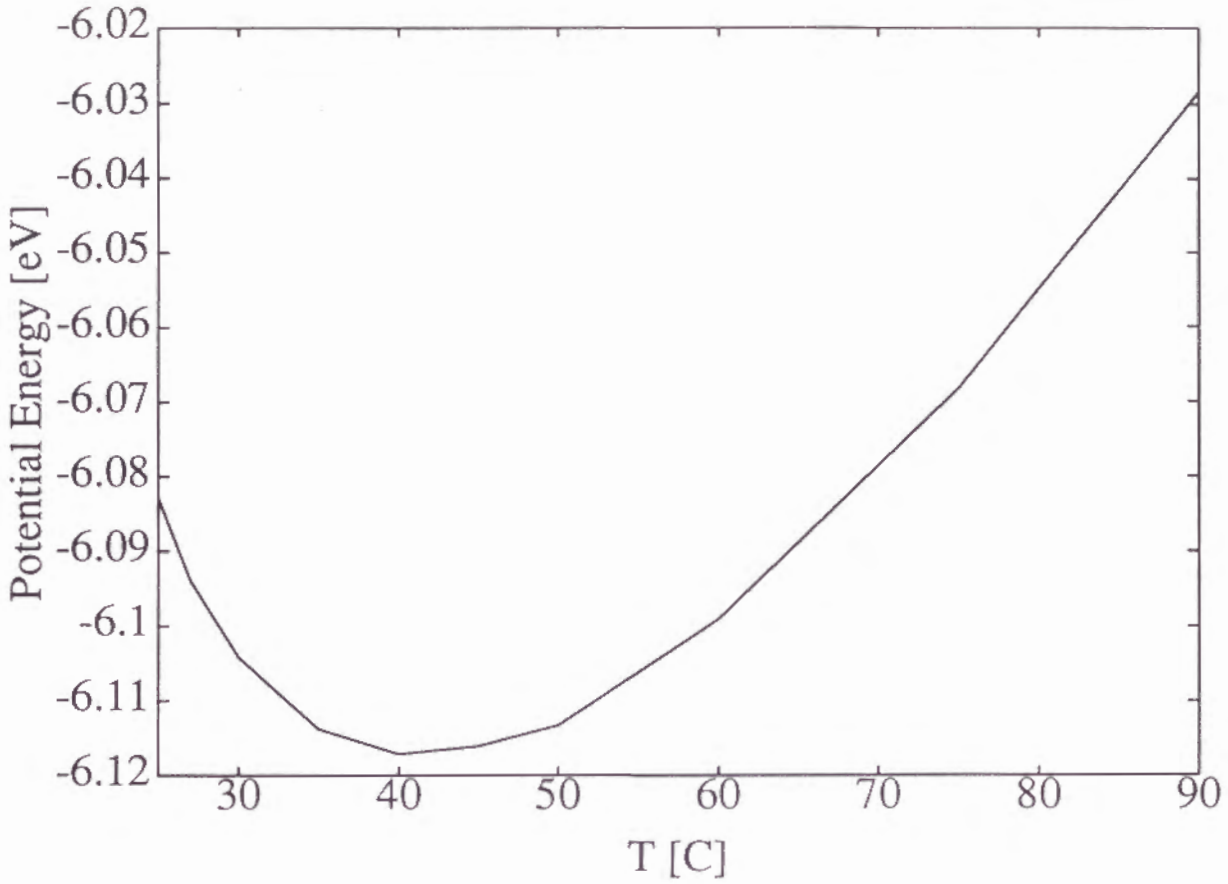
-6.02
-6.03
-6.04
-6.05
-6.06
-6.07
-6.08
-6.09
-6.1
-6.11
-6.12
Potential Energy [eV]
30
40
50
60
70
80
90
T [C]

Fig. 6 (b)

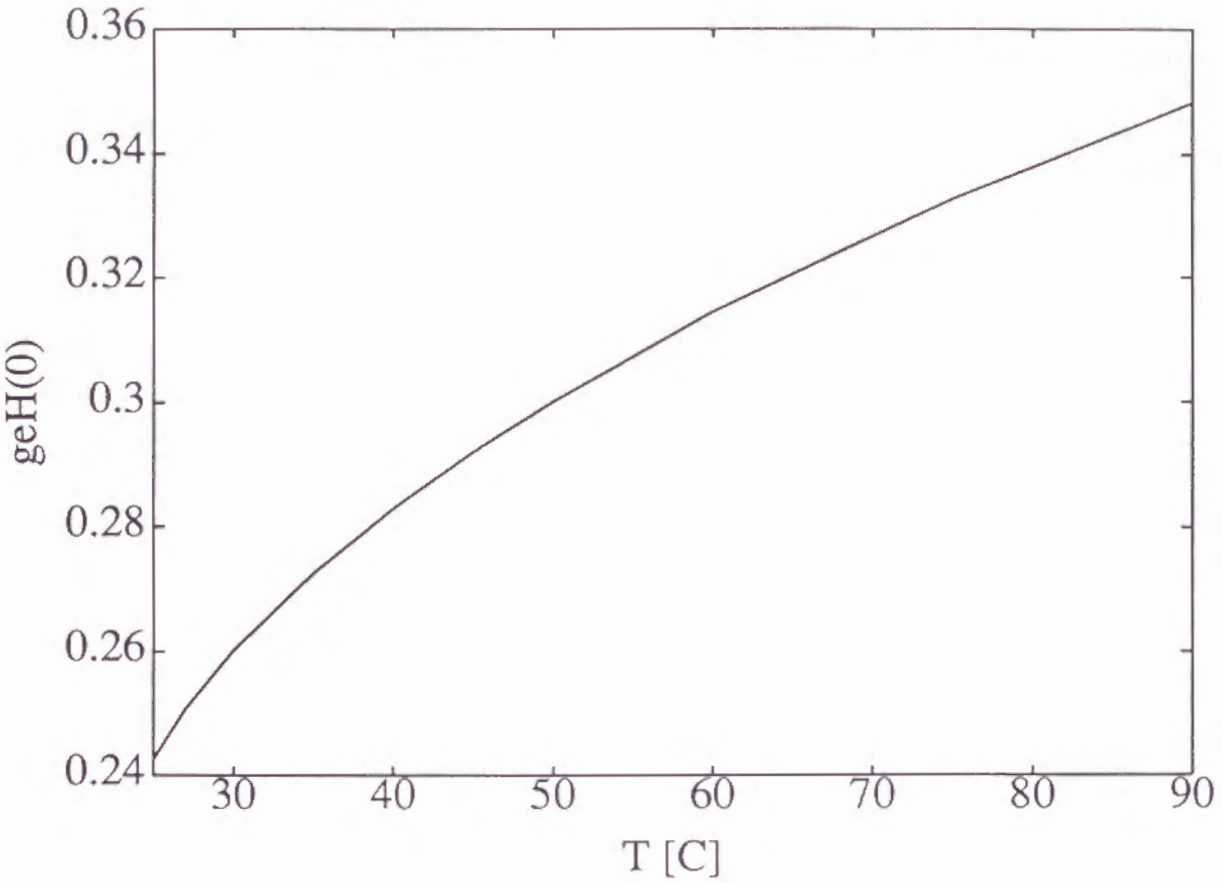

Fig. 7

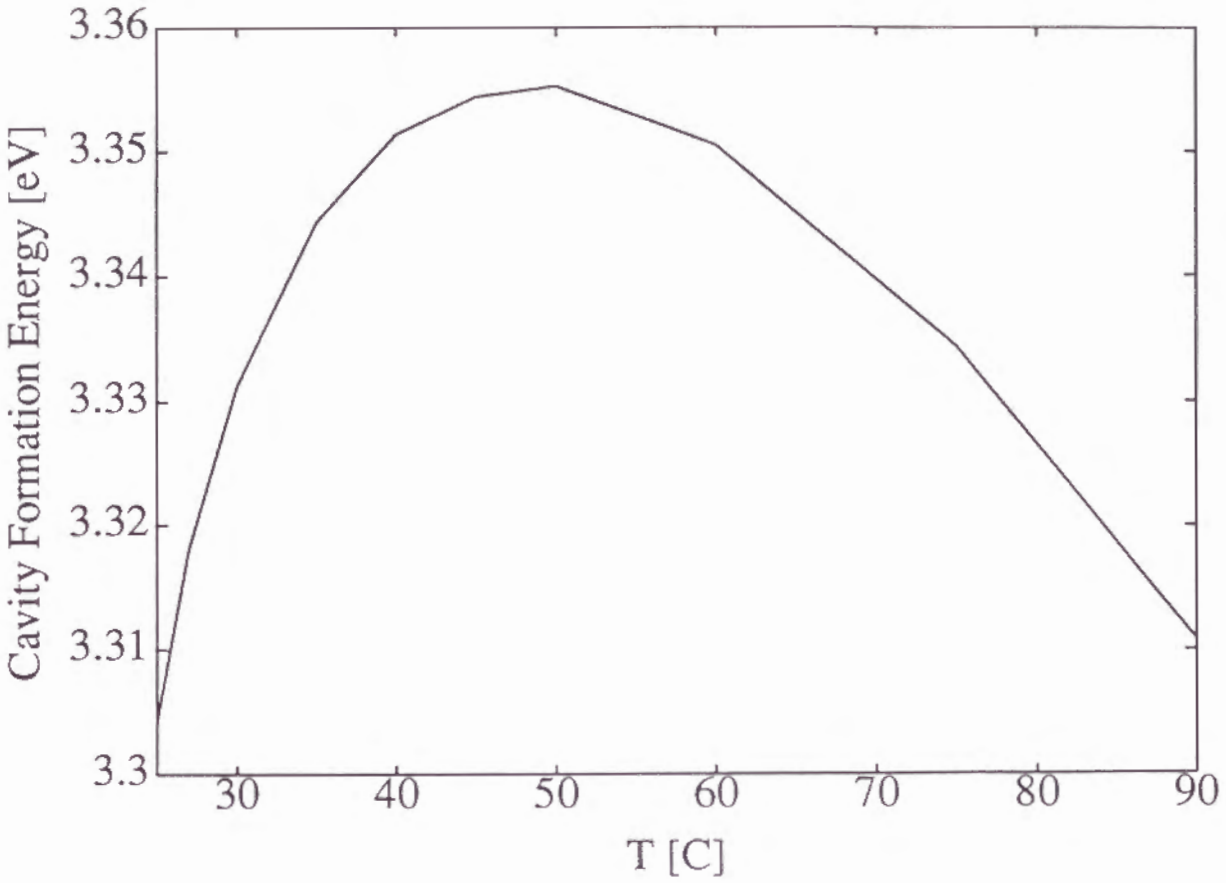
Cavity Formation Energy [eV]
3.36
3.35
3.34
3.33
3.32
3.31
3.3
30
40
50
60
70
80
90
T [C]

Fig. 8

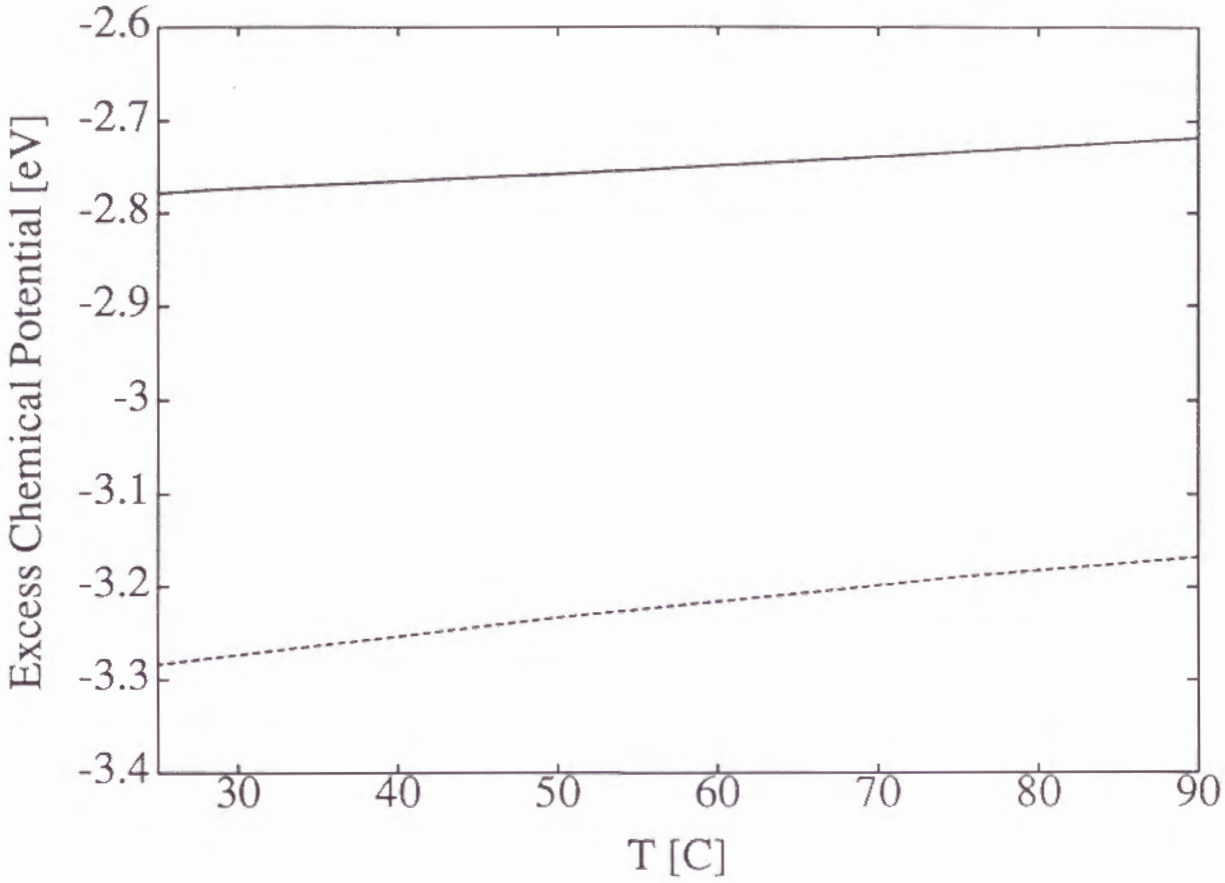
Excess Chemical Potential [eV]
-2.6
-2.7
-2.8
-2.9
-3
-3.1
-3.2
-3.3
-3.4
30
40
50
60
70
80
90
T [C]

Fig. 9

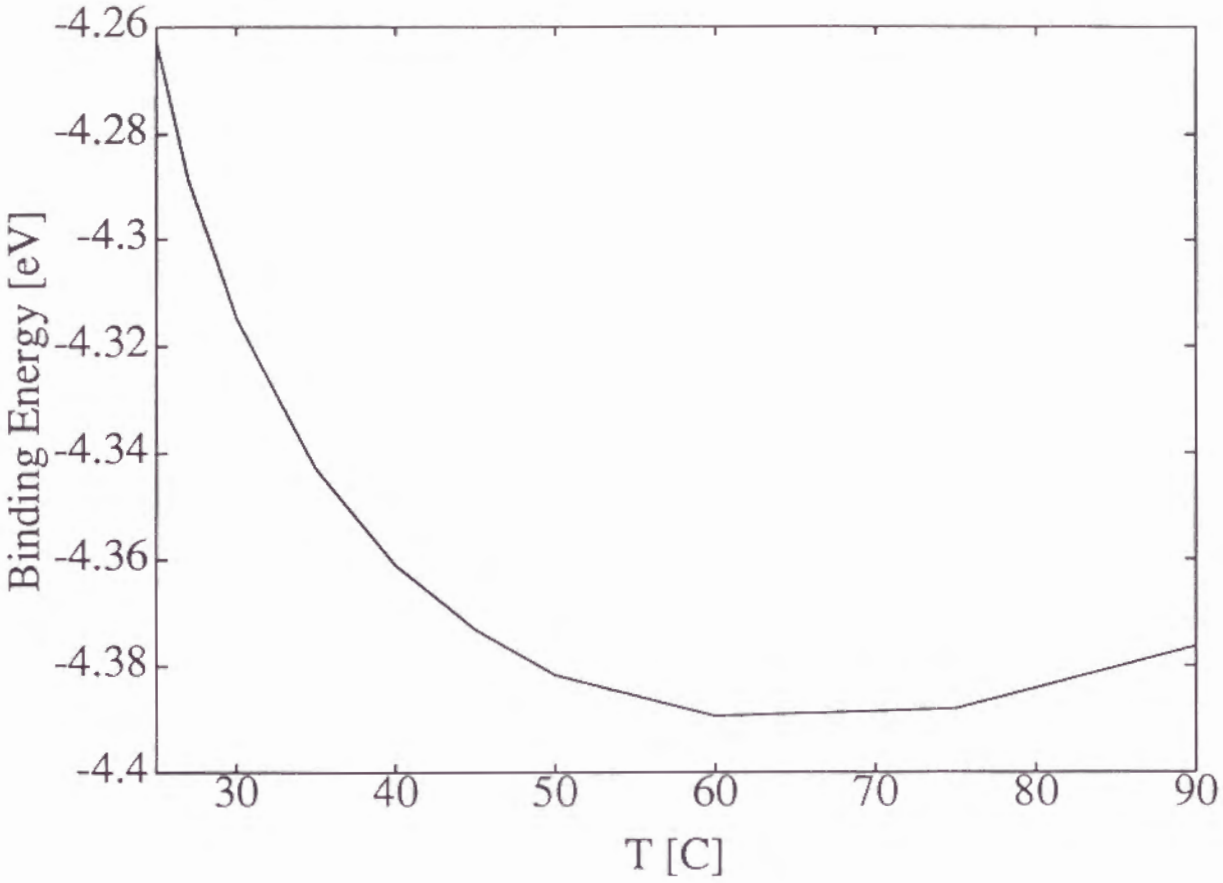
-4.26
-4.28
-4.3
-4.32
-4.34
-4.36
-4.38
-4.4
Binding Energy [eV]
30
40
50
60
70
80
90
T [C]

Fig. 10

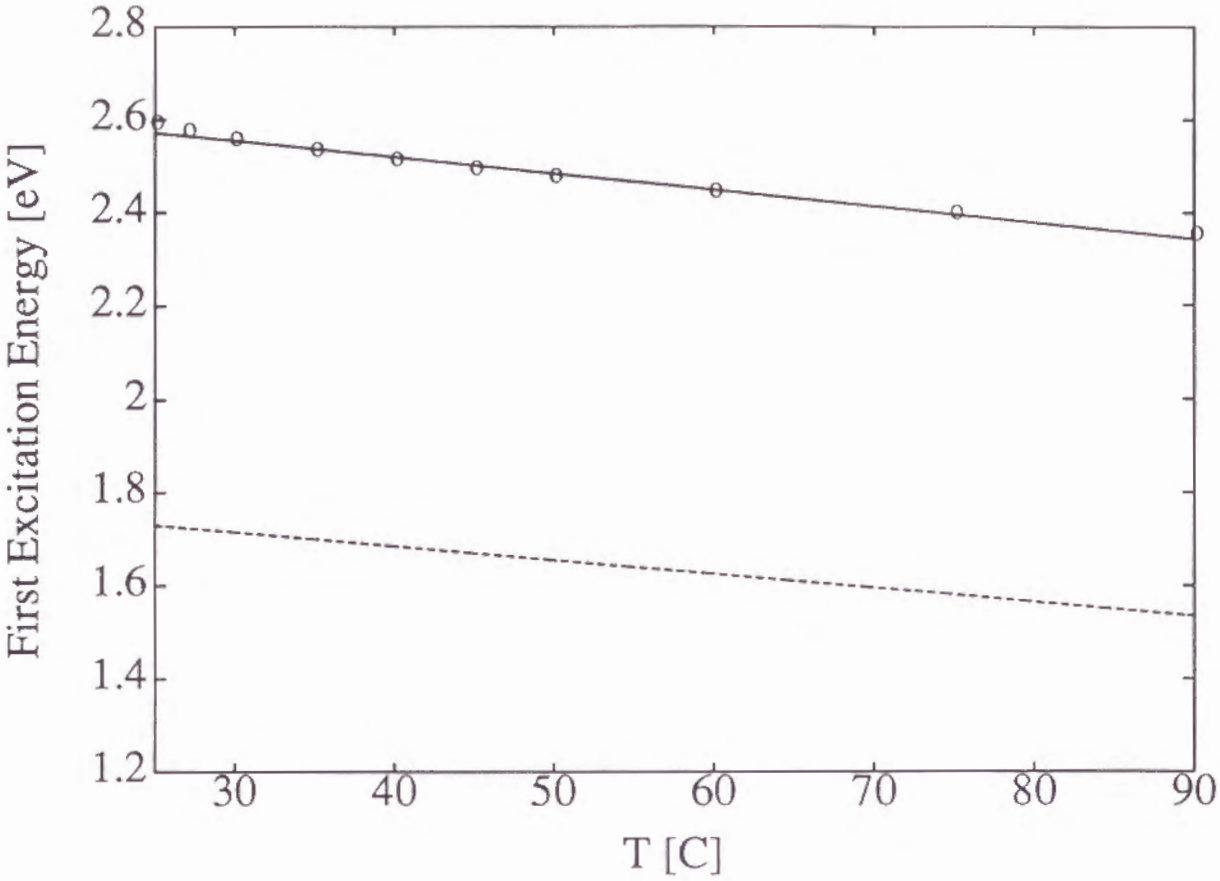
First Excitation Energy [eV]
2.8
2.6
2.4
2.2
2
1.8
1.6
1.4
1.2
30
40
50
60
70
80
90
T [C]

Fig. 11

III. Collective excitations in liquid water

This chapter is organized as follows. In III-1, definitions and notation used in this chapter are introduced. The collective modes on mass and charge density are determined by the Mori-Zwanzig formalism; limiting behavior of the eigen frequencies of collective modes is discussed in section III-2. The method of calculation and the condition of the MD simulation are described in III-3. Numerical results and discussions are presented in III-4.

III-1. Definitions and notation

A. Dynamical variable

First, we introduce an appropriately chosen set of dynamical variables to analyze the collective dynamical modes in polar liquids. In this paper, we are primarily concerned with the behavior of the system concerning the "acoustic" and "optical" character. A description of the system in terms of densities and currents of mass and charge is proper for this situation. To define the dynamical variables mentioned above, we employ the interaction site model (ISM) as a liquid model.[1] An ISM molecule is represented by a collection of interaction sites which usually stand for atoms in a molecule. The system may be regarded as a mixture of interaction sites. Hence we can define the site (or atomic) density and the associated current in molecular liquid. The Fourier component of the microscopic density of site is written as

$$\rho^{(\alpha)}(\mathbf{k},t)=\sum_{i=1}^{N}\exp\left[-i\mathbf{k}\cdot\mathbf{r}_i^{(\alpha)}(t)\right] \quad , \tag{1}$$

where N is the total number of molecules in the system, $\mathbf{r}_i^{(\alpha)}(t)$ is the position of the αth site of the ith molecule at time t, and the corresponding site current as

$$\mathbf{j}^{(\alpha)}(\mathbf{k},t) = \sum_{i=1}^{N} \mathbf{v}_i^{(\alpha)} \exp\left[-i\mathbf{k}\cdot\mathbf{r}_i^{(\alpha)}(t)\right] \quad , \tag{2}$$

where $\mathbf{v}_i^{(\alpha)}(t)$ is the velocity of the αth site of the ith molecule. For ISM liquid the densities of mass and charge can be expressed in terms of the site densities as

$$\rho_M(\mathbf{k},t) = \sum_{\alpha=1}^{n_s} m_\alpha \rho^{(\alpha)}(\mathbf{k},t) \quad , \tag{3a}$$

$$\rho_Z(\mathbf{k},t) = \sum_{\alpha=1}^{n_s} z_\alpha \rho^{(\alpha)}(\mathbf{k},t) \quad , \tag{3b}$$

where n_s is the number of sites in a molecule, and m_α and z_α denote the mass and charge of the αth site respectively. The associated currents are defined as

$$\mathbf{j}_M(\mathbf{k},t) = \sum_{\alpha=1}^{n_s} m_\alpha \mathbf{j}^{(\alpha)}(\mathbf{k},t) \quad , \tag{4a}$$

$$\mathbf{j}_Z(\mathbf{k},t) = \sum_{\alpha=1}^{n_s} z_\alpha \mathbf{j}^{(\alpha)}(\mathbf{k},t) \quad . \tag{4b}$$

The variable of charge density has been introduced to derive the dielectric function for ISM liquid, which takes account for the molecular structure explicitly.[2] It has properties similar to the variable of the collective polarization consisting of molecular dipoles[3] as the wavelength becomes long. On the other hand, the acoustic behavior of the system can be examined by the variable of mass density defined above as that of center-of-mass density. Former can describe a non-trivial contribution from the rotational motion to the acoustic mode naturally. At finite wavelength close to the intermolecular distance, the variables employed in our study are more proper than the traditional ones.

B. Time correlation function and power spectrum

The correlation of fluctuation in mass and charge densities is described by two autocorrelation functions respectively:

$$F_{MM}(\mathbf{k},t)=\frac{1}{N}\langle\rho_M(\mathbf{k},t)\rho_M(-\mathbf{k})\rangle=\sum_{\alpha=1}^{n_s}\sum_{\gamma=1}^{n_s}m_\alpha m_\gamma F_{\alpha\gamma}(\mathbf{k},t) \quad , \tag{5a}$$

$$F_{ZZ}(\mathbf{k},t)=\frac{1}{N}\langle\rho_Z(\mathbf{k},t)\rho_Z(-\mathbf{k})\rangle=\sum_{\alpha=1}^{n_s}\sum_{\gamma=1}^{n_s}z_\alpha z_\gamma F_{\alpha\gamma}(\mathbf{k},t) \quad , \tag{5b}$$

where $F_{\alpha\gamma}(\mathbf{k},t)$ is a site density correlation function (DCF) between site α and γ defined by

$$F_{\alpha\gamma}(\mathbf{k},t)=\frac{1}{N}\langle\rho_\alpha(\mathbf{k},t)\rho_\gamma(-\mathbf{k})\rangle \quad . \tag{6}$$

Both of mass and charge DCFs can be represented by the linear combination of the same site DCFs, however, coefficients of site DCFs are different. This could lead the qualitative difference in dynamics of mass and charge density.

Current correlation functions (CCFs) can be defined similarly. Since the current is a vector quantity, we separate it into its component parallel and perpendicular to the wavevector **k**. The longitudinal CCF defined by the correlation of the parallel component is written as

$$C^L_{MM}(\mathbf{k},t)=\frac{1}{N}\langle\mathbf{k}\cdot\mathbf{j}_M(\mathbf{k},t)\mathbf{k}\cdot\mathbf{j}_M(-\mathbf{k})\rangle=\sum_{\alpha=1}^{n_s}\sum_{\gamma=1}^{n_s}m_\alpha m_\gamma C^L_{\alpha\gamma}(\mathbf{k},t) \quad , \tag{7a}$$

$$C^L_{ZZ}(\mathbf{k},t)=\frac{1}{N}\langle\mathbf{k}\cdot\mathbf{j}_Z(\mathbf{k},t)\mathbf{k}\cdot\mathbf{j}_Z(-\mathbf{k})\rangle=\sum_{\alpha=1}^{n_s}\sum_{\gamma=1}^{n_s}z_\alpha z_\gamma C^L_{\alpha\gamma}(\mathbf{k},t) \quad , \tag{7b}$$

where $C^L_{\alpha\gamma}(\mathbf{k},t)$ is a longitudinal site CCF between site α and γ. The transverse CCF defined by the correlation of the perpendicular component is not discussed in this thsis.

To define a spectral function, we introduce the Fourier-Laplace transform of a function $f(k,t)$, (denoted by a tilde)

$$\tilde{f}(k,\omega)=\int_0^\infty f(k,t)e^{i\omega t}dt \quad , \tag{8}$$

and the Fourier transform

$$f(k,\omega)=\frac{1}{2\pi}\int_{-\infty}^{\infty} f(k,t)e^{i\omega t}dt=\frac{1}{\pi}\mathrm{Re}\,\tilde{f}(k,\omega) \quad . \tag{9}$$

In term of these definitions, the spectrum of fluctuation in density and current can be given. The correlation in density fluctuation is not independent of the correlation in the longitudinal current fluctuation, because the density is related to its current by equation of continuity. This gives relations as follows:[1]

$$C^{L}_{MM}(k,\omega)=\omega^2 S_{MM}(k,\omega) \quad , \tag{10a}$$

$$C^{L}_{ZZ}(k,\omega)=\omega^2 S_{ZZ}(k,\omega) \quad , \tag{10b}$$

where $S_{MM}(k,\omega)$ (or $S_{ZZ}(k,\omega)$) is the frequency spectrum of mass (or charge) density called dynamic structure factor. At the wavevector investigated by the MD simulation, the central and displaced peaks of the dynamic structure factor may merge into one continuous band so that we can no longer determine the frequency of density wave. This problem does not occur in the current fluctuation spectrum since it has a well-defined peak at any k. Hence we examine mainly the longitudinal current spectrum, not the dynamic structure factor.

Static structure factor is given by the autocorrelation function of density at time *0*

$$S_{MM}(k)=F_{MM}(k,0)=\sum_{\alpha=1}^{n_s}\sum_{\gamma=1}^{n_s} m_\alpha m_\gamma S_{\alpha\gamma}(k) \quad , \tag{11a}$$

$$S_{ZZ}(k)=F_{ZZ}(k,0)=\sum_{\alpha=1}^{n_s}\sum_{\gamma=1}^{n_s} z_\alpha z_\gamma S_{\alpha\gamma}(k) \quad , \tag{11b}$$

where $S_{\alpha\gamma}(k)$ is a site-site static structure factor between site α and γ.

III-2. Collective modes in polar liquids

In this section, we seek the eigen frequencies of collective modes for mass and

charge densities based on the projection operator formalism.[4] Amplitudes of each mode in mass and charge DCFs will be given.

A. Analysis based on projection operator formalism

We choose a dynamical vector consisting of mass and charge densities

$$\rho(\mathbf{k},t)=\begin{bmatrix}\rho_M(\mathbf{k},t)\\ \rho_Z(\mathbf{k},t)\end{bmatrix} \quad . \tag{12}$$

In terms of the dynamical vector a correlation function matrix can be defined by

$$\mathbf{F}(k,t)=\left\langle \rho(\mathbf{k},t)\rho^{\dagger}(\mathbf{k})\right\rangle=\begin{bmatrix}F_{MM}(k,t) & F_{MZ}(k,t)\\ F_{ZM}(k,t) & F_{ZZ}(k,t)\end{bmatrix} \tag{13}$$

where $F_{MZ}(k,t)$ denotes a cross correlation function between mass and charge density. The correlation function matrix obeys the generalized Langevin equation

$$\dot{\mathbf{F}}(k,t)+i\Omega\cdot\mathbf{F}(k,t)+\int_0^t\mathbf{M}(k,t-s)\cdot\mathbf{F}(k,s)ds=\mathbf{0} \quad , \tag{14}$$

where $\mathbf{M}(k,t)$ is the memory function matrix which is defined by the correlation function matrix of a random force vector. In our case the frequency matrix Ω whose elements are proportional to the cross correlation between $\rho_{M,Z}(\mathbf{k},0)$ and $\dot{\rho}_{M,Z}(\mathbf{k},0)$ is identically zero, because the site position dose not correlate with the site velocity in the equilibrium.[5] In turn the memory function matrix satisfies the equation

$$\dot{\mathbf{M}}(k,t)+\int_0^t\mathbf{N}(k,t-s)\cdot\mathbf{M}(k,s)ds=\mathbf{0} \quad , \tag{15}$$

where $\mathbf{N}(k,t)$ is a second-order memory function matrix.

The solution of Eq. (14) in terms of the Fourier-Laplace transform can be written with substituting Eq (15) as

$$\tilde{\mathbf{F}}(k,\omega)=\left[-i\omega\mathbf{I}+\left[-i\omega\mathbf{I}+\tilde{\mathbf{N}}(k,\omega)\right]^{-1}\cdot\mathbf{M}(k,0)\right]^{-1}\cdot\mathbf{F}(k,0) \quad , \tag{16}$$

where $\mathbf{I}$ is a unit matrix. Since we are primarily concerned with the expression of the eigen frequencies of collective modes, in a first approximation the damping can

be neglected, that is to say, $\tilde{\mathbf{N}}(k,\omega)$ is set to zero. Eq. (16) becomes

$$\tilde{\mathbf{F}}(k,\omega)=\left[-i\omega\mathbf{I}+\frac{1}{-i\omega}\mathbf{M}(k,0)\right]^{-1}\cdot\mathbf{F}(k,0) \quad . \tag{17}$$

We can determine the eigen frequencies by solving the secular equation

$$\det\left[\omega^2\mathbf{I}-\mathbf{M}(k,0)\right]=0 \quad . \tag{18}$$

The matrix elements of $\mathbf{M}(k,0)$ which is the memory function matrix at time *0* are written as

$$\begin{aligned}\mathbf{M}(k,0)&=\begin{bmatrix}M_{11}(k) & M_{12}(k)\\ M_{21}(k) & M_{22}(k)\end{bmatrix}\\ &=\begin{bmatrix}\langle\dot{\rho}_M(\mathbf{k})\dot{\rho}_M(-\mathbf{k})\rangle/N & \langle\dot{\rho}_M(\mathbf{k})\dot{\rho}_Z(-\mathbf{k})\rangle/N\\ \langle\dot{\rho}_Z(\mathbf{k})\dot{\rho}_M(-\mathbf{k})\rangle/N & \langle\dot{\rho}_Z(\mathbf{k})\dot{\rho}_Z(-\mathbf{k})\rangle/N\end{bmatrix}\begin{bmatrix}S_{MM}(k) & S_{MZ}(k)\\ S_{ZM}(k) & S_{ZZ}(k)\end{bmatrix}^{-1} \quad .\end{aligned} \tag{19}$$

The detailed expression of kinetic factor $\langle\dot{\rho}(\mathbf{k})\dot{\rho}(-\mathbf{k})\rangle/N$ is given elsewhere.[6] This expression is dependent on the structure of an ISM molecule. The solution of Eq. (18) can be written as

$$\omega^2_{M,Z}=\frac{1}{2}\left\{M_{11}(k)+M_{22}(k)\pm\sqrt{\left(M_{22}(k)-M_{11}(k)\right)^2+4M_{12}(k)M_{21}(k)}\right\} \quad , \tag{20}$$

where the eigen frequency with suffix M (or Z) corresponds to that of - (or +) in braces. When mass and charge densities are independent each other [i.e., $M_{12}(k)=M_{21}(k)=0$], the squares of the eigen frequencies coincide with the reduced second moments of $S_{MM}(k,\omega)$ and $S_{ZZ}(k,\omega)$, $\omega_0^2(k)$ and $\omega'^2_0(k)$, respectively. That is to say, $\omega_0(k)$ (or $\omega'_0(k)$) gives the characteristic frequency of mass (or charge) fluctuation in the case of no coupling. The moments of spectral function are given by the short time expansion of the correlation function as shown in Appendix A.

We can obtain the DCFs of mass and charge within our non-damping approximation. The functions $F_{MM}(k,t)$ and $F_{ZZ}(k,t)$ which are the diagonal elements of the correlation function matrix can be written by means of inverse Fourier-Laplace transform as

$$F_{MM}(k,t) = S_{MM}(k)\{A_{MM}(k)\cos\omega_M t + A_{MZ}(k)\cos\omega_Z t\} \quad , \tag{21a}$$

$$F_{ZZ}(k,t) = S_{ZZ}(k)\{A_{ZM}(k)\cos\omega_M t + A_{ZZ}(k)\cos\omega_Z t\} \quad , \tag{21b}$$

where $A_{MM}(k)$, $A_{MZ}(k)$, $A_{ZM}(k)$, and $A_{ZZ}(k)$ are the amplitudes of the eigen modes in DCFs, which are given in Appendix B. By definition

$$A_{MM}(k) + A_{MZ}(k) = A_{ZM}(k) + A_{ZZ}(k) = 1 \quad . \tag{22}$$

If the $A_{MZ}(k)$ is zero, in time domain the $F_{MM}(k,t)$ oscillates by the frequency ω_M and in frequency domain $S_{MM}(k,\omega)$ consists of two delta functions located at $\pm\omega_M$. If not zero, in frequency domain $S_{MM}(k,\omega)$ consists of four delta functions located at $\pm\omega_M$ and $\pm\omega_Z$. This is a manifestation of the coupling between two eigen modes in dynamics of mass density. The structure of $S_{ZZ}(k,\omega)$ can be discussed similarly.

B. Limiting behavior of eigen frequencies

Here, we investigate the long wavelength limit of eigen frequencies given by Eq. (20). Since the explicit expressions of eigen frequencies are dependent on the molecular model as pointed out above, we apply limiting operation to the eigen frequencies for SPC water model.[7] However, we believe that the resultant limiting expressions hold for any polar liquids. In the small k limit, the eigen frequency of mass mode behaves as[1,8]

$$\omega_M^2(k) \approx \frac{k_B T}{M S_{\alpha\gamma}(0)} k^2 = v_T^2 k^2 \quad (k \to 0) \quad , \tag{23}$$

where k_B is the Boltzman constant, T is the absolute temperature of the system, M is the total mass of molecule, and v_T is the isothermal sound velocity. At long wavelength limit, all of site-site static structure factors are coincident.[1] In the case of charge density, limiting expression can be written as[3,6]

$$\omega_Z^2(k) \approx \frac{8\pi\rho\mu^2}{3I^*} \frac{\varepsilon}{\varepsilon - 1} = \omega_d^2 \quad (k \to 0) \quad , \tag{24}$$

where ρ is the number density of liquid, μ is the dipole moment of molecule, I^* is the average moment of inertia perpendicular to the dipolar axis and ε is the static dielectric constant. The collective mode of charge density is characterized by ω_d called dipolaron frequency.[3] This expression is equivalent to that of Stockmayer fluid which consists of dipoles embedded in spherical particle interacting with the Lennard-Jones potential.[9] However, k-dependence of charge mode is different due to molecular structure.

III-3. Computational details

The MD simulation of a system composed of 256 water molecules was carried out using the program MDMPOL developed by Smith and Fincham.[10] The program generates the trajectory of the system imposed cubic periodic boundary condition obeying Newtonian classical mechanics (NVE ensemble). The molecular geometry and parameters defining the intermolecular interaction were taken from SPC model.[7] The short-range interaction was truncated by the half of the MD box length, whereas the long range electrostatic interaction was included by means of the Ewald summation technique. The density of the system was fixed at 1.0 g/cm^3 and the mean temperature was 303.5 K. After the equilibration period, the simulation was extended to 712 ps with the integration time step of 0.5 fs. The trajectory was saved on disk every 3 fs. The time interval determines the upper limit of frequency that can be studied. The short interval chosen by us is due to the fast dynamics of charge density. The time correlation functions sampled with every fourth point of trajectory as time origin and evaluated up to about 20 ps.

To compute the static structure factors and time correlation functions, we have to introduce the wavevector **k**. In the simulation the wavevectors were restricted to have the values

$$\mathbf{k} = \frac{2\pi}{L}(n,m,l) \quad , \tag{25}$$

where n, m, l = 0, 1, ... , 12 and L= 19.712 Å was the side length of the MD box. For the calculation of time correlation functions, we selected the wavevector which satisfied the condition of $k = 2\pi p/L$ (p = 1, ... , 12). In an isotropic fluid, correlation functions do not depend on the direction of **k**, so that they were averaged over all equivalent **k**. The spectra of time correlation function were estimated by the numerical Fourier transform of Filon's method.[11]

III-4. Results and discussion

A. Static structure factors

In order to calculate the eigen frequencies and to estimate the intensities of the collective modes, we evaluated the static structure factors (SSFs). Fig. 1 shows the SSFs obtained by the MD calculation. The mass-mass SSF $S_{MM}(k)$ has a first peak between 2 and 3 Å^{-1}. This peak comes mainly from correlation between oxygen-oxygen (O-O) pair, and oxygen-hydrogen (O-H) pair adds small contribution, because mass of oxygen is about 16 times larger than that of hydrogen. For charge density, the overall charge neutrality of the system requires that $\lim_{k\to 0} S_{ZZ}(k) = 0$. The intensity of $S_{ZZ}(k)$ is enlarged with progression of k. Around 2 Å^{-1}, O-H pair makes large negative contribution and cancels the correlation of O-O pair. As a result, the first peak is given at larger wavevector ≈ 3 Å^{-1} than that of the peak of $S_{MM}(k)$. The

position of the peak in $S_{ZZ}(k)$ is determined by the period of oscillation of mean charge density around a reference molecule, whereas that in $S_{MM}(k)$ is determined by the value of nearest-neighbor distance. For simple charged liquid like molten salt, the main peak in $S_{ZZ}(k)$ usually occurs at a smaller value of k than that in $S_{MM}(k)$.[12] This is because the characteristic length of charge density is larger than the nearest-neighbor distance owing to the regular alternation of concentric shells of oppositely charged ions. For liquid water, the wavelength giving the first peak of $S_{ZZ}(k)$ corresponds to the length related to the hydrogen bonding between water molecules. This implies that the hydrogen bonding makes small wavelength oscillation of mean charge density in comparison with the intermolecular distance.

B. Eigen frequencies

In Fig. 2 (a) we show $\omega_0(k)$ and $\omega'_0(k)$, which correspond to the eigen frequencies of mass and charge modes with no coupling, respectively.[6] For the mass mode, frequency increases linearly at small wavevector as k increases and its slope gives the isothermal sound velocity $\approx$ 1411 m/s, which is good agreement with the experimental result.[13] Around 2 Å^{-1}, the frequency gives a minimum owing to the liquid structure. At higher wavevector, $\omega_0(k)$ is convergent to the ideal gas limit. In the case of the charge mode, the eigen frequency at small k limit is given by Eq. (3.13) $\approx$ 98 ps^{-1}. With increasing k, the charge mode shows marked negative dependence on k or negative dispersion. The minimum originating from the peak of $S_{ZZ}(k)$ is located at about 3 Å^{-1}. After passing minimum, charge mode converges on the ideal gas limit. The square of the eigen frequencies with no coupling can be given by the sum of the two contributions; one comes from the translation of

molecules and the other from the rotation of molecules. Each contribution in $\omega_0^2(k)$ and $\omega'^2_0(k)$ is exhibited in Fig. 2 (b) and (c). The mass mode is dominated by the translational motion of molecules for all k examined and the rotational motion of molecules gives small contribution. The charge mode is mainly determined by rotational motion. Translational motion gives minor, but growing contribution with increasing k.

In Fig. 3 (a) two eigen frequencies of the system with considering the coupling are depicted. The eigen frequency of mass mode has little difference compared to $\omega_0(k)$. In the case of charge mode, however, the eigen frequency is considerably renormalized and is shifted to higher frequency. The amplitude of each mode in $F_{MM}(k,t)$ and $F_{ZZ}(k,t)$ is also shown in Fig. 3 (b). At k = 0, $A_{MM}(0) = A_{ZZ}(0) = 1$ [i.e., $A_{MZ}(0) = A_{ZM}(0) = 0$], which means that two modes are completely decoupled. With increasing k, $A_{MM}(k)$ remains almost one, that is, charge mode gives little influence on the mass fluctuation all over the k investigated by us. On the other hand, the amplitude of charge mode in $F_{ZZ}(k,t)$, $A_{ZZ}(k)$, decreases rapidly above the wavevector 1.0 Å^{-1}. In other words, the amplitude of mass mode in $F_{ZZ}(k,t)$, $A_{ZM}(k) = 1 - A_{ZZ}(k)$, grows markedly at nearly 1.0 Å^{-1}. Our results suggest that at $k > 1.0$ Å^{-1} the coupling between mass and charge fluctuation occurs and the translational motion changes the dynamics of charge fluctuation remarkably. We will discuss the origin of this behavior in the following sections on the basis of the results of the MD simulation.

C. Density correlation functions

Fig. 4 shows the normalized autocorrelation functions of mass and charge densities. For mass density, the relaxation time of DCF first decreases with k, but

then shows a marked increase at k = 1.91 Å^{-1} which is the wavevector close to the main peak in $S_{MM}(k)$. This phenomenon is widely known as the de Gennes slowing down effect [14], which is caused by the strong spatial correlation of mass density. At larger wavevector, the relaxation time decreases again and approaches the ideal gas limit. In Fig. 5 we show the mass DCFs divided into two contributions, self and distinct parts. The former corresponds to the single molecule correlation and the latter to the intermolecular correlation. At k = 0.319 Å^{-1} two contributions are almost equal in magnitude and opposite in sign so that they are canceled to a large extent each other. With increasing k, the distinct part is reduced and the contribution from the self part increases. At k = 1.91 Å^{-1} where $F_{MM}(k,t)$ shows the slowing down, the dynamics of mass density is almost determined by the self part. Hence at k > 1.9 Å^{-1} the mass fluctuation is dominated by the single molecule correlation. For charge density, at the smallest wavevector the relaxation of charge fluctuation is much faster than that of mass fluctuation and $F_{ZZ}(k,t)$ shows oscillatory behavior up to 0.4 ps with the following slow tail. As seen in next section, the initial oscillation is related to the collective librational motion of water molecules. The oscillation in $F_{ZZ}(k,t)$ diminishes accompanied by the slowing down of correlation function as k increases. At high k, both of mass and charge DCFs behave similarly except that the charge fluctuation shows faster initial decay than the mass fluctuation. In Fig. 5 we show the charge DCFs divided into the self and distinct parts. At k = 0.319 Å^{-1} two parts are also almost equal in magnitude and opposite in sign. As a result, $F_{ZZ}(k,t)$ shows rapid initial decay. The initial oscillatory behavior comes mainly from the distinct part and the residual slow contribution can be attributed to the self part. As the wavevector increases, the distinct part in $F_{ZZ}(k,t)$ decreases, which leads the

reduction of the oscillatory behavior. The contribution from the self part increases with progression of k, which gives the slower tail in the charge DCF.

To make the situation clearer, we show the quantity related to the correlation time, the zero frequency component of the normalized dynamic structure factor, [15]

$$\frac{S(k,0)}{S(k)} = \frac{1}{\pi}\int_0^\infty \frac{F(k,t)}{S(k)}dt \quad . \tag{26}$$

This is proportional to a wavevector-dependent relaxation time $\tau_0(k)$ when the correlation function decays by the form of a simple exponential function $\exp[-t/\tau_0(k)]$. In our case, decay of density correlation does not obey the exponential form, however, we regard this quantity as an indicator of the correlation time. In Fig. 6 (a) our results are exhibited. For mass density, the relaxation time shows marked increase at k = 1.91 Å^{-1}, which is caused by the de Gennes slowing down effect discussed above. For charge density, the decay time grows above k = 1.0 Å^{-1} and gives a maximum at k = 1.91 Å^{-1} where the mass fluctuation shows marked slowing down. However, this is not caused by the strong spatial correlation of charge density because the peak of $S_{ZZ}(k)$ is located at nearly 3 Å^{-1}. Fig. 6 (b) and (c) depict the correlation times of the mass and charge DCFs divided into the self and distinct parts. Constituents of the mass and charge DCFs' relaxation times have similar tendency. The reduction of the contribution from the distinct part gives a maximum of the total correlation time. At k > 1.9 Å^{-1} the contribution from the distinct part is almost zero so that the relaxation times of density fluctuations in mass and charge are determined by the single molecule correlation. These facts suggest that around this wavevector the relaxation process of the charge fluctuation except the initial time regime is closely related to that of the mass fluctuation so that the slow tail in $F_{ZZ}(k,t)$ is given by the translational contribution in the self correlation. To confirm

this statement, we show the spectral functions in next section.

D. Optical dynamics

The spectra of longitudinal charge current are exhibited in Fig. 7. At the smallest k, a sharp peak is located at nearly 160 ps^{-1}, which can be attributed to the oscillation in $F_{ZZ}(k,t)$. This is related to the librational motion of water molecule concerning the axis of the smallest moment of inertia.[16,17] With increasing k, the peak moves toward lower frequency and the amplitude of the spectrum in the low frequency region increases, which is characterized by the translational motion of water molecules. At k = 2.55 $Å^{-1}$ we can recognize a distinct new peak located at the same frequency of the peak in $C^L_{MM}(k,\omega)$ shown in next section. To make the origin of the low frequency structure clear, we show the charge current spectra divided into the self and distinct parts in Fig. 8. At the smallest k the high frequency peak in $C^L_{ZZ}(k,\omega)$ is mainly ascribed to the distinct part. The lower frequency region of the self part is canceled by the distinct part. Above the wavevector 1.27 $Å^{-1}$, the shape of the self part is almost independent of k, which has the low frequency peak at nearly 10 ps^{-1}. The wavevector dependence of the structure of the total spectrum is determined by that of the distinct part. At k = 1.27 $Å^{-1}$, the low frequency region in the self part is almost canceled by the distinct part and the residual contribution from the self part makes the low frequency structure in $C^L_{ZZ}(k,\omega)$. With increasing k, the distinct part is reduced, which gives the low frequency structure originating from the self correlation. We can, therefore, conclude that above the wavevector 1.0 $Å^{-1}$ the charge fluctuation is coupled to the translational mode through the single molecule motion, which provides the slow tail in $F_{ZZ}(k,t)$. This behavior plays an

important role to describe the solvation dynamics of small ions because the large wavevector components of $C_{ZZ}^{L}(k,\omega)$ contribute to the solvation process, which may give the slow tail in solvation time correlation functions. It is noted that $C_{ZZ}^{L}(k,\omega)$ calculated by the quasianalytical integral equation theory devised to include the single molecule character is reported.[18] Their theory predicts the additional structure in spectra especially at $k > 2$ Å^{-1} as shown in our results. The additional peak, however, appears at much higher frequency in comparison with mass mode. Their theory indicates at least that the single molecule motion plays an important role to describe the polarization charge fluctuation near the wavelength close to the intermolecular distance. This point agrees with our opinion. The dispersion relation for charge mode is obtained from the peak position of the longitudinal current spectrum. The resultant peak frequencies, $\omega_{CZ}(k)$, are shown in Fig. 9. The characteristic frequencies $\omega'_0(k)$ and $\omega_{LO}(k)$ which is the square root of the reduced second moment of $C_{ZZ}^{L}(k,\omega)$ defined in Appendix A are also presented. Unfortunately, there is no explicit expression of $\omega_{LO}(k)$ for ISM liquid so that we obtained that from the short time behavior of current correlation function numerically. We call the square root of the reduced second moment of current spectrum the phonon frequency by the analogy with lattice dynamics. The peak frequencies, $\omega_{CZ}(k)$, are well characterized by the phonon frequency of the optical mode, $\omega_{LO}(k)$ at $k < 1.5$ Å^{-1}. This feature is known for more simple charged liquid as molten salt.[1] However, for liquid water, the value of $\omega_{LO}(k)$ is much larger than that of $\omega'_0(k)$ by about 50 %, for molten salt, 20-30 % larger. This can be attributed to the strong short-range interaction between water molecules. The difference between $\omega_{CZ}(k)$ and $\omega_{LO}(k)$ might be due to the coupling between mass and charge current as shown for density

fluctuations in section B.

E. Acoustic dynamics

The spectra of longitudinal mass current are depicted in Fig. 10. To concentrate on the collective dynamics, the mass current spectra at the wavevector k < 1.5 Å^{-1} are shown. At k = 0.319 Å^{-1} there is a sharp peak in low frequency region of $C^{L}_{MM}(k,\omega)$, which corresponds to sound mode. With increasing k, the peak moves toward higher frequency. At k = 1.27 Å^{-1} we can see an additional low frequency structure in the spectrum. To clarify the origin of this structure, we show the spectrum divided into the self and distinct parts in Fig. 11. At k = 0.319 Å^{-1} the peak of the self part is reinforced by that of the distinct part each other. With increasing k, the peak frequency in the distinct correlation is shifted to higher frequency, which gives the peak of the total spectrum. The structure of the self part is almost independent of k, but this is canceled by the negative contribution from the distinct part. As the large wavevector increases, the distinct part is reduced, which provides the low frequency structure in $C^{L}_{MM}(k,\omega)$. The dispersion relation for mass mode is depicted in Fig. 12.

The characteristic frequencies $\omega_0(k)$ and $\omega_{LA}(k)$ are also presented. At k < 1.5 Å^{-1}, the peak frequencies increase linearly with k and its slope gives the velocity of mass density wave ≈ 3502 m/s. This value agrees with the "fast sound" velocity reported in the previous works.[5,19-24] If this mode corresponds to the new excitation which is distinct from the normal sound, the two peaks should be exist in spectra. In our simulation, there is only one peak in spectrum simultaneously at any k.[5,22,24] The low frequency structure of the spectrum at k >1.0 Å^{-1} is caused by the self correlation

so that this does not correspond to the collective excitation as sound mode. Hence our results support that the high sound velocity can be attributed to the continuous positive dispersion from normal sound wave.[8] This problem will be discussed in the next section based on the viscoelastic theory. At $k > 1.9$ Å^{-1} the peak frequency approaches $\omega_0(k)$, which characterizes the single molecule dynamics.

F. Modeling of longitudinal current spectra

In this section, we discuss what determines the peak frequency of the longitudinal current spectrum. For this purpose we look for a more detailed phenomenological description of density or current fluctuation based on the memory function formalism.[4] For simplicity, we do not consider the coupling between mass and charge fluctuation explicitly. We begin by writing a continued fraction expansion of $F_{MM}(k,t)$ in the form

$$\tilde{F}_{MM}(k,\omega) = \frac{S_{MM}(k)}{-i\omega + \dfrac{\omega_0^2(k)}{-i\omega + \Delta\tilde{n}_2(k,\omega)}} \quad , \tag{27}$$

where

$$\Delta = \omega_{LA}^2(k) - \omega_0^2(k) \quad . \tag{28}$$

and $n_2(k,t)$ is an unknown memory function. This is entirely equivalent to writing

$$\tilde{C}_{MM}(k,\omega) = \frac{\omega_0^2(k) S_{MM}(k)}{-i\omega + \dfrac{\omega_0^2(k)}{-i\omega} + \Delta\tilde{n}_2(k,\omega)} \quad . \tag{29}$$

This is the exact expression up to the fourth moment of the dynamic structure factor irrespective of the form of the memory function. We introduce a simplest approximation for $n_2(k,t)$ given by the exponential form

$$n_2(k,t) = \exp\left(-\frac{t}{\tau(k)}\right) \quad , \tag{30}$$

where $\tau(k)$ is an unknown wavevector-dependent relaxation time. This assumption is equivalent to introducing the Maxwellian-type relaxation of the viscosity; the limit $\omega\tau(k) << 1$ corresponds to viscous flow, while the limit $\omega\tau(k) >> 1$ corresponds to elastic wave, so that we call this model the viscoelastic model.[1,8] With this assumption the longitudinal current spectrum can be written as

$$C_{MM}(k,\omega) = \frac{1}{\pi} \frac{\omega_0^2(k) S_{MM}(k) \Delta\tau(k) \omega^2}{\left(\omega^2 - \omega_0^2(k)\right)^2 + \left(\omega\tau(k)\left(\omega^2 - \omega_{LA}^2\right)\right)^2} \quad . \tag{31}$$

The associated dispersion relation is given by the physical solutions of the following equation:

$$2\left(\omega^2\right)^2 \left\{\omega^2 - \omega_{LA}^2(k)\right\} + \left(\frac{1}{\tau(k)}\right)^2 \left\{\left(\omega^2\right)^2 - \left(\omega_0^2(k)\right)^2\right\} = 0 \quad . \tag{32}$$

Here, we investigate two limiting solutions of Eq. (32).[25] At small k, both of $\omega_0(k)$ and $\omega_{LA}(k)$ vanish as k^2, whereas $\left(1/\tau(k)\right)^2$ remains having finite value. In this case, the approximate solution can be given by $\omega_{CM}^2(k) \approx \omega_0^2(k)$. This model gives the ordinary hydrodynamic result at small k. We call this case the viscous limit. On the other hand, at higher wavevector, using the fact that $\omega_{LA}^2(k)$ is often distinctly larger than $\omega_0^2(k)$, the approximate solutions can be written by

$$\omega_{CM}^2(k) \approx \omega_{LA}^2(k) - \frac{1}{2}\left(\frac{1}{\tau(k)}\right)^2 \quad . \tag{33}$$

In any case, with increasing k from hydrodynamic limit, the peak frequency of $C_{MM}^L(k,\omega)$ moves from the hydrodynamic results $\omega_0(k)$ upward to higher frequency, which approaches $\omega_{LA}(k)$ in the case of relatively long relaxation time. If the frequencies considered are much larger than the relaxation rate $1/\tau(k)$, the system responds with the frequency $\omega_{LA}(k)$ which characterizes the solidlike response. We call this case the elastic limit. Consequently, $\omega_{CM}(k)$ has an intermediate value

between two limits, the viscous limit and the elastic limit. The actual value of $\omega_{CM}(k)$ is determined by the efficiency of the relaxation process of $n_2(k,t)$. To derive the dispersion relation based on the viscoelastic model, we need the time constant $\tau(k)$. We obtained $\tau(k)$ by the least-square fitting of simulation results using Eq. (31). The spectra calculated by the viscoelastic model are shown in Fig. 10. The overall structure of spectrum is well reproduced. The optimized relaxation rate is shown in Fig. 13. At $k < 1.5$ Å^{-1}, the shear relaxation rate is close to the peak frequency so that the relaxation rate in in between the viscous limit and the elastic limit. This implies that the mass fluctuation shows "viscoelastic" behavior in the time scale characterized by the inverse of $\omega_{CM}(k) \approx$ a few subpicoseconds. As seen in Fig. 12 the peak frequency $\omega_{CM}(k)$ is well described by our model. In the case of liquid water, the peak frequency is very large in comparison with $\omega_0(k)$, which may have misled us to the existence of the new collective excitation, "fast sound". However, $\omega_{CM}(k)$ still has smaller value compared to $\omega_{LA}(k)$. That is to say, anomaly in liquid water lies in the unexpected large value of $\omega_{LA}(k)$.[25] This can be ascribed to the strong short-range interaction between water molecules. We can conclude that the high sound velocity is a consequence of the continuous positive dispersion of the normal sound.

For charge current we can adapt the phenomenological model used to describe the mass current spectrum. The resultant expression for $C_{ZZ}^{L}(k,\omega)$ is identical to Eq. (31) except that $S_{ZZ}(k)$ replaces $S_{MM}(k)$, $\omega'_0(k)$ replaces $\omega_0(k)$, $\omega_{LO}(k)$ replaces $\omega_{LA}(k)$ and a new relaxation time $\tau'(k)$ replaces $\tau(k)$. The spectra obtained by a least-square adjustment of $\tau'(k)$ are shown in Fig. 7. Qualitative feature is reproduced, however, the peak position is incorrect at small k. A consideration of coupling between mass

and charge current will give an improvement of the peak position. A fit is not good at high wavevector because of the additional peak originating from the mass mode. As shown in Fig. 13, the shear relaxation rate is smaller than the peak frequency, so that Eq. (33) is good approximation. Therefore, the charge fluctuation shows "elastic" behavior in the time scale characterized by the inverse of $\omega_{CZ}(k) \approx$ some ten femtoseconds. That is why the polarization charge fluctuation at small k shows oscillatory behavior nearly by the frequency $\omega_{LO}(k)$.

Appendix A

In this appendix, we give the short time expansion of time correlation functions and the moments of spectral functions. First, we expand the density correlation function in a Taylor series as follows:[1]

$$F_{MM}(k,t) = S_{MM}(k)\left\{1 - \omega_0^2(k)\frac{t^2}{2!} + \omega_0^2(k)\omega_{LA}^2(k)\frac{t^4}{4!} - \cdots\right\} \quad , \tag{A1a}$$

$$F_{ZZ}(k,t) = S_{ZZ}(k)\left\{1 - \omega_0'^2(k)\frac{t^2}{2!} + \omega_0'^2(k)\omega_{LO}^2(k)\frac{t^4}{4!} - \cdots\right\} \quad , \tag{A1b}$$

where

$$\omega_0^2(k) = \frac{1}{N}\frac{\langle \dot{\rho}_M(k)\dot{\rho}_M(-k)\rangle}{S_{MM}(k)} \quad , \tag{A2a}$$

$$\omega_0'^2(k) = \frac{1}{N}\frac{\langle \dot{\rho}_Z(k)\dot{\rho}_Z(-k)\rangle}{S_{ZZ}(k)} \quad , \tag{A2b}$$

and

$$\omega_0^2(k)\omega_{LA}^2(k) = \frac{1}{N}\frac{\langle \ddot{\rho}_M(k)\ddot{\rho}_M(-k)\rangle}{S_{MM}(k)} \quad , \tag{A3a}$$

$$\omega_0'^2(k)\omega_{LO}^2(k) = \frac{1}{N}\frac{\langle \ddot{\rho}_Z(k)\ddot{\rho}_Z(-k)\rangle}{S_{ZZ}(k)} \quad , \tag{A3b}$$

are the reduced second and fourth frequency moments of $S_{MM}(k,\omega)$ (or $S_{ZZ}(k,\omega)$), respectively. The subscripts LA ("longitudinal acoustic") and LO ("longitudinal optic") are introduced in analogy with the language of phonons. The reduced second frequency moments can be expressed in terms of static correlation function and molecular parameters, however, detailed expression is dependent on the molecular model. For reduced fourth moment there is no explicit expression for ISM liquid. We can expand the longitudinal current correlation function similarly. The reduced second moment of the longitudinal mass (or charge) current correlation function is equivalent to $\omega_{LA}^2(k)$ (or $\omega_{LO}^2(k)$).

Appendix B

Here, we derive the explicit expression of the $F_{MM}(k,t)$ and $F_{ZZ}(k,t)$ with our non-damping theory. The correlation function matrix of Eq. (17) can be written with Laplace variable $s = -i\omega$

$$\tilde{\mathbf{F}}(k,s) = \left[s\mathbf{I} + \frac{1}{s}\mathbf{M}(k,0) \right]^{-1} \cdot \mathbf{F}(k,0) \quad . \tag{B1}$$

The mass density correlation function is

$$\tilde{F}_{MM}(k,s) = \frac{s}{(s-s_M^2)(s-s_Z^2)} \left\{ (s^2 + M_{22}(k)) S_{MM}(k) - M_{12}(k) S_{ZM}(k) \right\} \quad , \tag{B2}$$

where s_M and s_Z are the solutions of secular equation. Eq (B2) can be split into the sum of two terms as follows:

$$\begin{aligned} \tilde{F}_{MM}(k,s) = \frac{s}{s_M^2 - s_Z^2} \{ & \frac{s_M^2 S_{MM}(k) + M_{22}(k) S_{MM}(k) - M_{12}(k) S_{ZM}(k)}{s^2 - s_M^2} \\ & - \frac{s_Z^2 S_{MM}(k) + M_{22}(k) S_{MM}(k) - M_{12}(k) S_{ZM}(k)}{s^2 - s_Z^2} \} \quad . \end{aligned} \tag{B3}$$

By means of inverse Laplace transform, we obtain $F_{MM}(k,t)$ as

$$\begin{aligned} F_{MM}(k,t) = & \frac{-\omega_M^2 S_{MM}(k) + M_{22}(k) S_{MM}(k) - M_{12}(k) S_{ZM}(k)}{\omega_Z^2 - \omega_M^2} \cos\omega_M t \\ & - \frac{-\omega_Z^2 S_{MM}(k) + M_{22}(k) S_{MM}(k) - M_{12}(k) S_{ZM}(k)}{\omega_Z^2 - \omega_M^2} \cos\omega_Z t \quad . \end{aligned} \tag{B4}$$

By Eq. (B4) we can get Eq. (21a) with an obvious definition of $A_{MM}(k)$ and $A_{MZ}(k)$. Similarly we can obtain the expression of $F_{ZZ}(k,t)$

$$\begin{aligned} F_{ZZ}(k,t) = & \frac{-\omega_M^2 S_{ZZ}(k) + M_{11}(k) S_{ZZ}(k) - M_{21}(k) S_{MZ}(k)}{\omega_Z^2 - \omega_M^2} \cos\omega_M t \\ & - \frac{-\omega_Z^2 S_{ZZ}(k) + M_{11}(k) S_{ZZ}(k) - M_{21}(k) S_{MZ}(k)}{\omega_Z^2 - \omega_M^2} \cos\omega_Z t \quad . \end{aligned} \tag{B5}$$

By definition

$$A_{MM}(k) + A_{MZ}(k) = A_{ZM}(k) + A_{ZZ}(k) = 1 \quad . \tag{B6}$$

At $k = 0$ limit, the mass and charge density fluctuation is completely decoupled as

$$A_{MM}(0) = A_{ZZ}(0) = 1 \quad . \tag{B7}$$

Reference

[1] J. P. Hansen and I. R. McDonald, *Theory of simple liquids,* 2nd edition (Academic Press, London, 1990).

[2] F. O. Raineri, Y. Zhou, H. L. Friedman and G. Stell, Chem. Phys. **152**, 201 (1991).

[3] P. Madden and D. Kivelson, Adv. Chem. Phys. **56**, 467 (1984), and references therein.

[4] H. Mori, Prog. Theor. Phys. **33**, 423 (1965); ibid. **34**, 399 (1965)

[5] M. A. Ricci, D. Rocca, G. Ruocco and R. Vallauri, Phys. Rev. A **40**, 7226 (1989).

[6] H. Resat, F. O. Reineri and H. L. Friedman, J. Chem. Phys. **97**, 2618 (1992).

[7] H. J. C. Berendsen, J. P. M. Postma, W. F. V. Gunsteren and J. Hermans, In *Intermolecular Forces*, edited by B. Pullman (Reidel, Dordrecht, 1981), p 331.

[8] J. P. Boon and S. Yip, *Molecular hydrodynamics* (McGraw-Hill, New York, 1980).

[9] E. L. Pollock and B. J. Alder, Phys. Rev. Lett. **46**, 950 (1981).

[10] W. Smith and D. Fincham, CCP5 Newsletter, an informal letter freely available from Science & Research Council, Daresbury Laboratory, Warrington WA4 4AD, England.

[11] M. P. Allen and D. J. Tildesley, *Computer simulation of liquids*, (Clarendon Press, Oxford, 1987).

[12] J. P. Hansen and I. R. McDonald, Phys. Rev. A **11**, 2111 (1975).

[13] J. Teixeira and J. Leblond, J. Phys. Lett., **39**, L83 (1978).

[14] P. G. DeGennes, Physica **25**, 825 (1959).

[15] M. Dixon, Phil. Mag. B **47**, 531 (1983).

[16] F. Hirata and P. J. Rossky, J. Chem. Phys. **74**, 6867 (1981).

[17] D. Bertolini, A. Tani and R.Vallauri, Mol. Phys. **73**, 69 (1991); ibid. **75**, 1047 (1992).

[18] H. Resat, F. O. Reineri and H. L. Friedman, J. Chem. Phys. **98**, 7277 (1993).

[19] A. Rahman and F. H. Stillinger, Phys. Rev. A **10**, 368 (1974).

[20] R. W. Impey, P. A. Madden and I. R. McDonald, Mol. Phys. **46**, 513 (1982).

[21] J. Teixeira, M. C. Bellissent-Funel, S. H. Chen and B. Dorner, Phys. Rev. Lett. **54**, 2681 (1985).

[22] M. Wojcik and E. Clementi, J. Chem. Phys. **85**, 6085 (1986).

[23] T. Kowall, P. Mausbach and A. Geiger, Ber. Bunsenges. Phys. Chem., **94**, 279 (1990).

[24] F. Sciortino and S. Sastry, J. Chem. Phys. **100**, 3881 (1994).

[25] U. Balucani, G. Ruocco, A. Torcini and R. Vallauri, Phys. Rev. E **47**, 1677 (1993).

Figure captions

Fig. 1: Static structure factors for mass-mass (a) and charge-charge (b) correlation. Solid line, total correlation; dashed line, O-O pair; dashdot line, O-H pair; dotted line, H-H pair.

Fig. 2: (a): Square root of the reduced second moment of dynamic structure factor for charge density (upper branch) and for mass density (lower branch). Dashed line stands for the ideal gas limit. (b) and (c): $\omega_0^2(k)$ and $\omega'^2_0(k)$ are divided into the contribution from translation and rotation of molecules. (b) and (c) correspond to mass and charge mode, respectively. Solid line, contribution from translational motion; dashed line, that from rotational motion.

Fig. 3: (a): Eigen frequencies of mass (lower branch) and charge (upper branch) mode. Solid line, with coupling between mass and charge density; dashed line, without coupling. (b): Amplitude of each mode in density correlation functions. Solid line, $A_{MM}(k) = 1 - A_{MZ}(k)$; dashed line, $A_{ZZ}(k) = 1 - A_{ZM}(k)$.

Fig. 4: Selected results of normalized density correlation functions for $k = 2\pi p / L$ (p = 1, 4, 6, 8), where L= 19.712 Å. Solid line, mass-mass; dashed line, charge-charge correlation.

Fig. 5: Selected results of the normalized density correlation functions divided into self and distinct parts for mass-mass (upper panel) and charge-charge (lower panel).

Solid line, self part; dashed line, distinct part.

Fig. 6: Zero frequency component of normalized dynamics structure factors. Solid line, mass-mass; dashed line, charge-charge correlation. (a); Divided into self and distinct parts for mass-mass (b) and for charge-charge (c) correlation. Solid line, self part; dashed line, distinct part. Circles are molecular dynamics results and the line is drawn as an aid to the eye.

Fig. 7: Selected results of charge current spectra for $k = 2\pi p/L$ (p = 1, 4, 7, 8). Circles, the simulation results; solid line, fitted results obtained by Eq. (31). Notice that the angular frequency $\omega = 100$ ps^{-1} is equivalent to ≈ 530 cm^{-1}.

Fig. 8: Selected results of charge current spectra for $k = 2\pi p/L$ (p = 1, 4, 7, 8). Solid line, total correlation; dashed line, self part; dotted line, distinct part.

Fig. 9: Dispersion relation for charge mode. Upper solid line, phonon frequency of optical mode; lower solid line, square root of the reduced second moment of dynamic structure factor; dashed line, dispersion relation obtained from Eq. (32) with the optimized relaxation time; circles, peak frequency of current fluctuation spectrum.

Fig. 10: Selected results of mass current spectra for $k = 2\pi p/L$ (p = 1, 2, 3, 4). Circles, the simulation results; solid line, fitted results obtained by Eq. (31).

Fig. 11: Selected results of mass current spectra for $k = 2\pi p/L$ (p = 1, 2, 3, 4). Solid

line, total correlation; dashed line, self part; dotted line, distinct part.

Fig. 12: Dispersion relation for mass mode. Upper solid line, phonon frequency of acoustic mode; lower solid line, square root of the reduced second moment of dynamic structure factor; dashed line, dispersion relation obtained from Eq. (32) with the optimized relaxation time; circles, peak frequency of current fluctuation spectrum; stars, peak frequency of self part.

Fig. 13: The inverse of the optimized relaxation time. Solid line for mass mode; dashed line for charge mode, circles, peak frequency of mass current spectrum; stars, peak frequency of charge current spectrum.

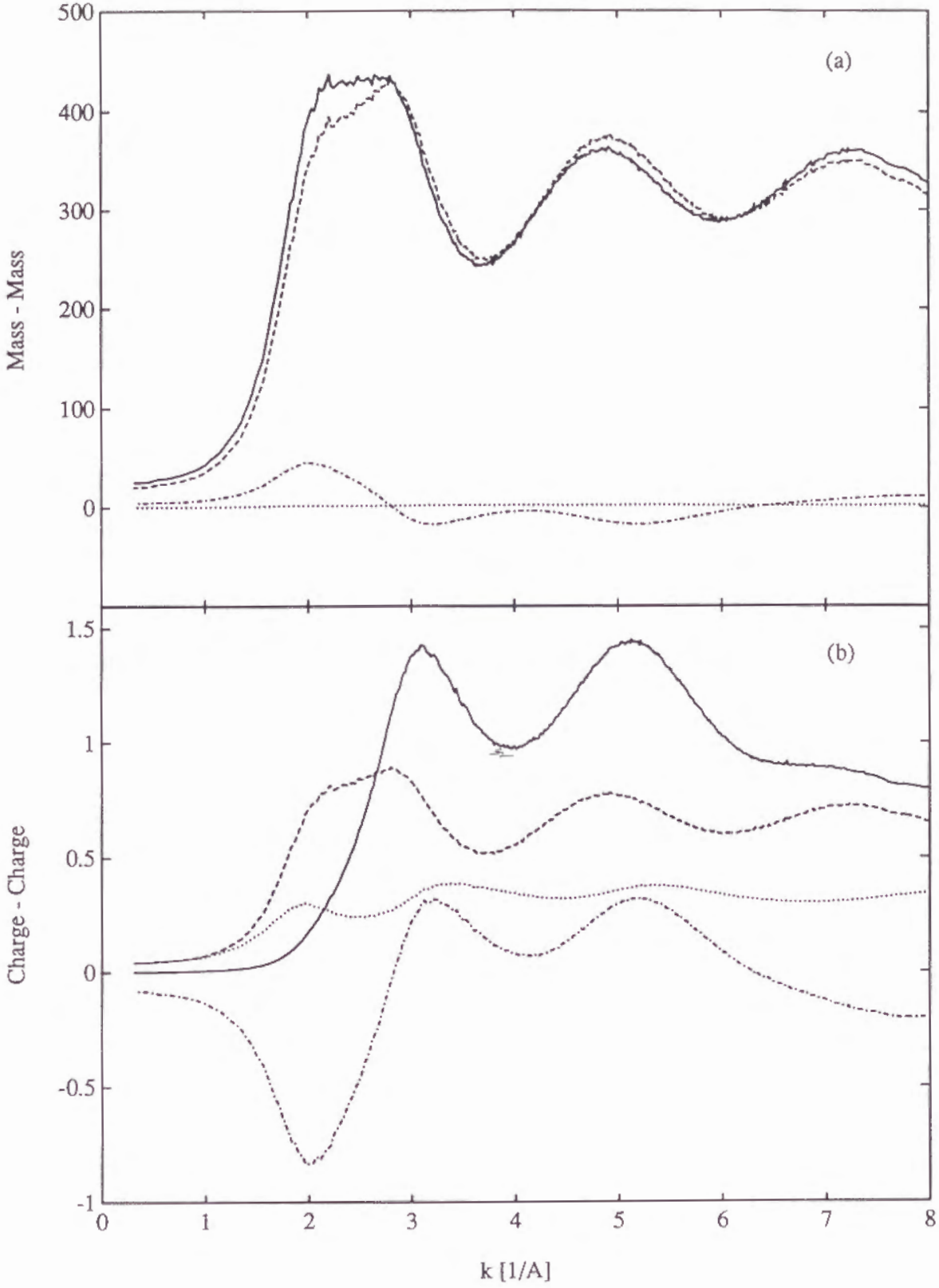
(a)
(b)
Mass - Mass
Charge - Charge
k [1/A]
500
400
300
200
100
0
1.5
1
0.5
0
-0.5
-1
0
1
2
3
4
5
6
7
8

Fig. 1

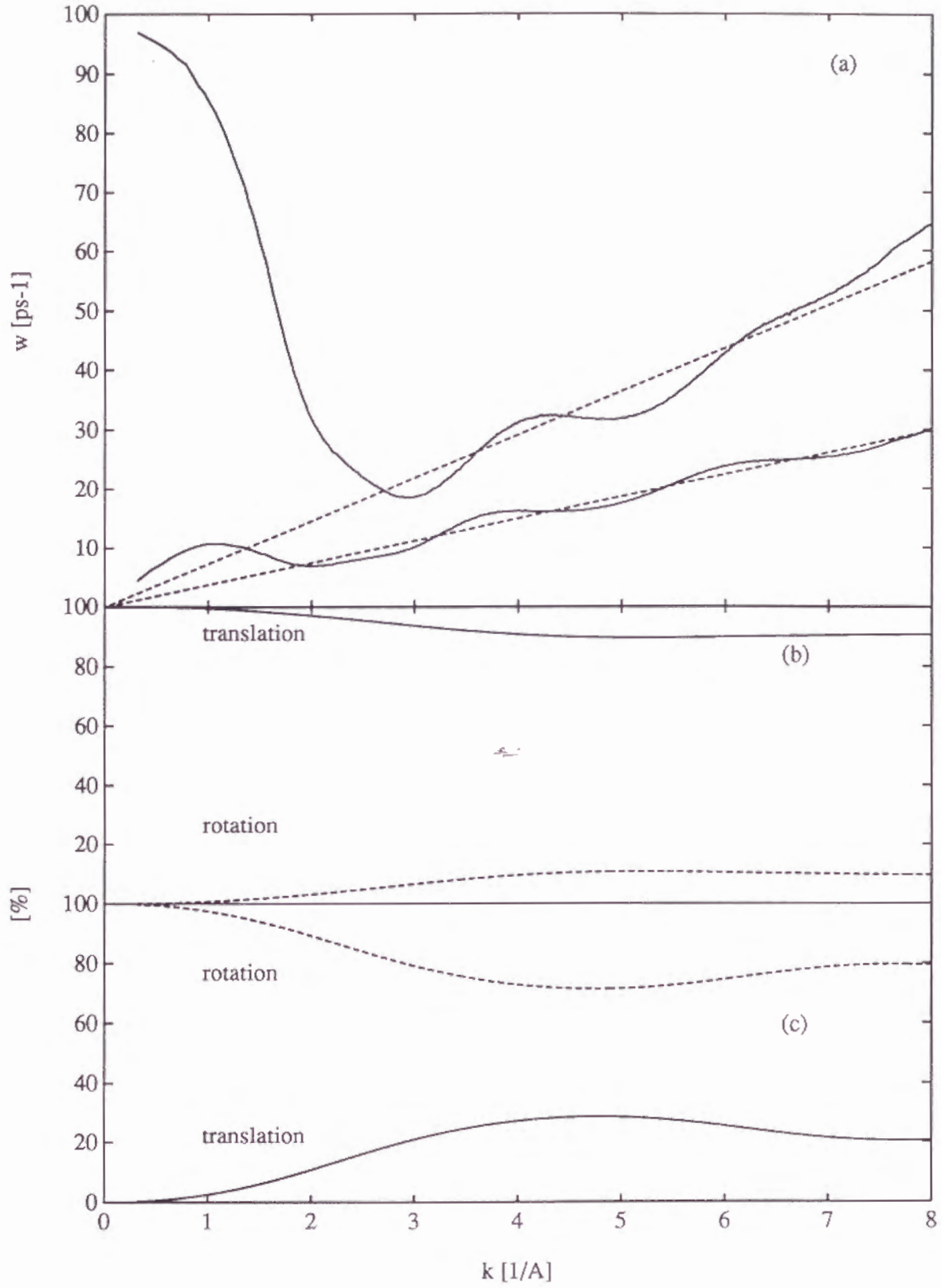

Fig. 2

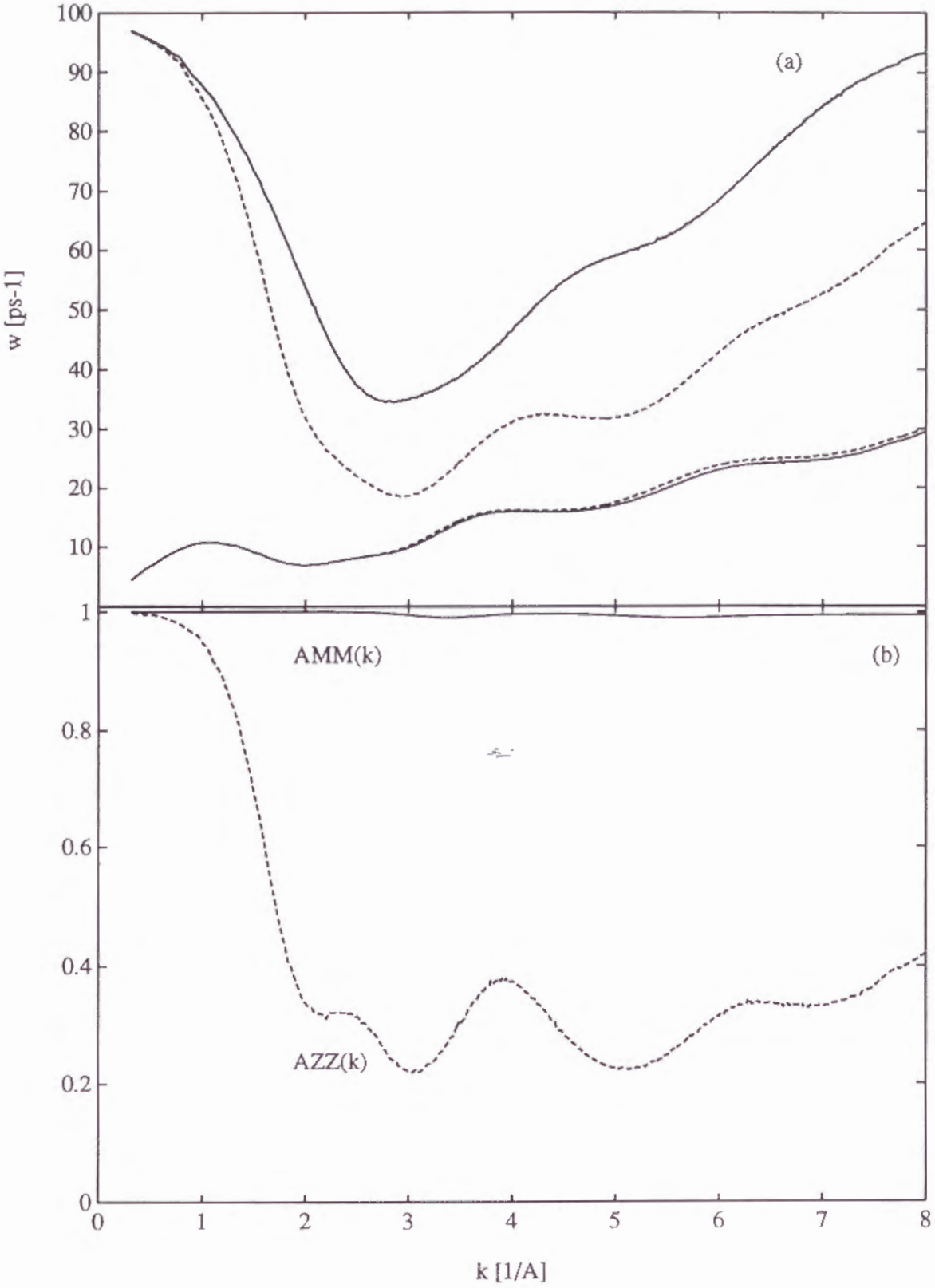

Fig. 3

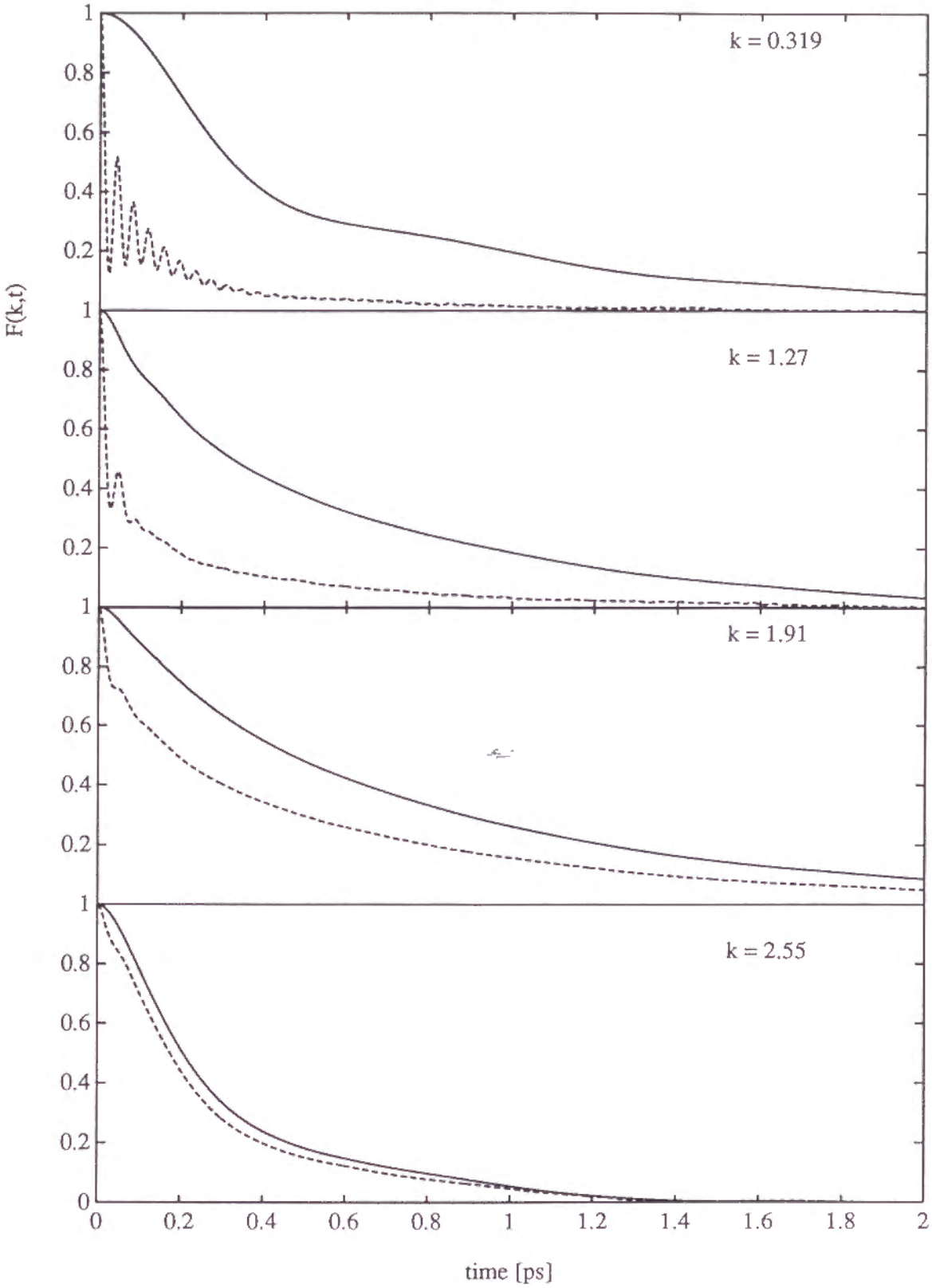

Fig. 4

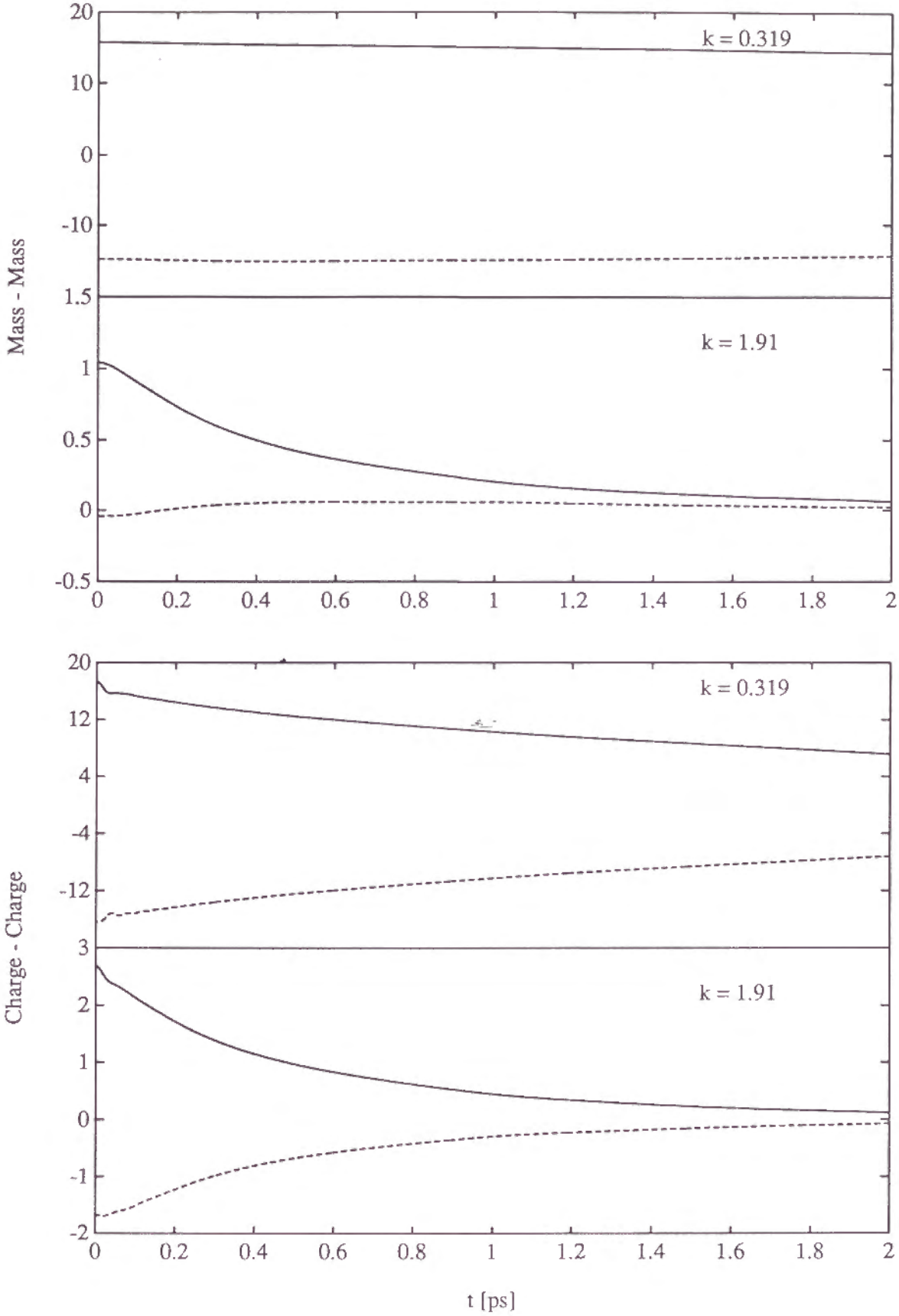

Fig. 5

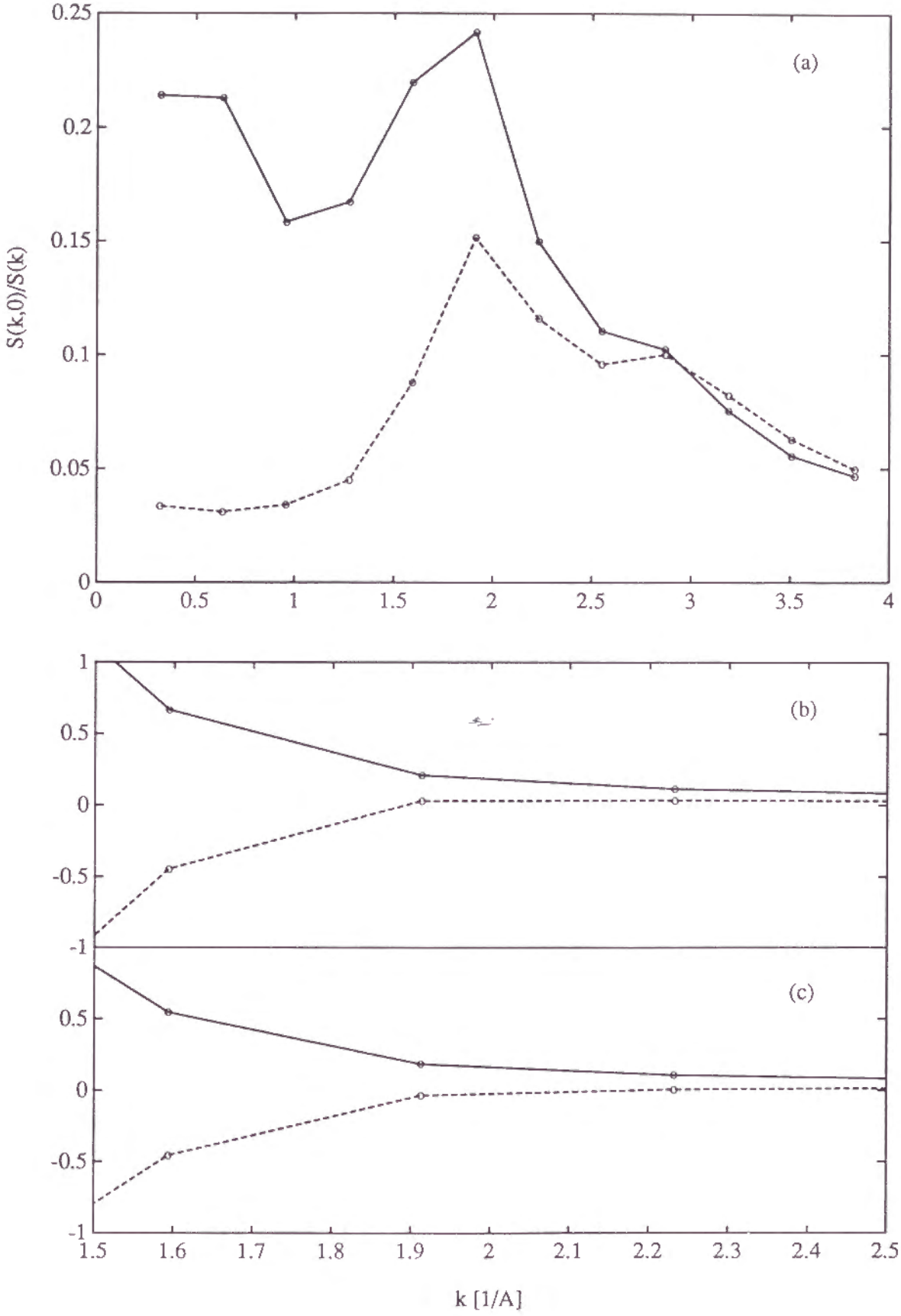

Fig. 6

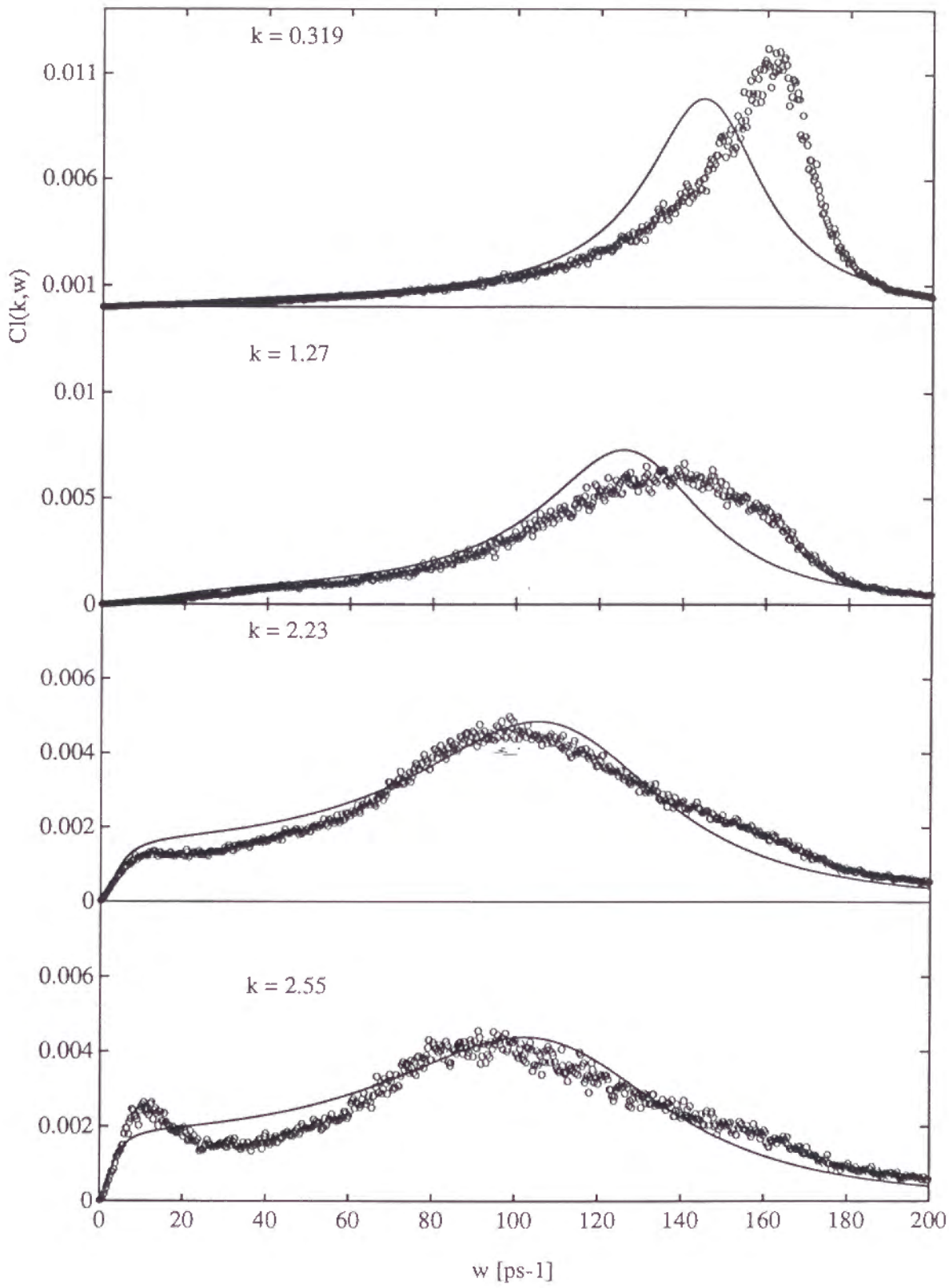
k = 0.319
k = 1.27
k = 2.23
k = 2.55
Cl(k,w)
w [ps-1]
0.011
0.006
0.001
0.01
0.005
0
0.004
0.002
0
20
40
60
80
100
120
140
160
180
200

Fig. 7

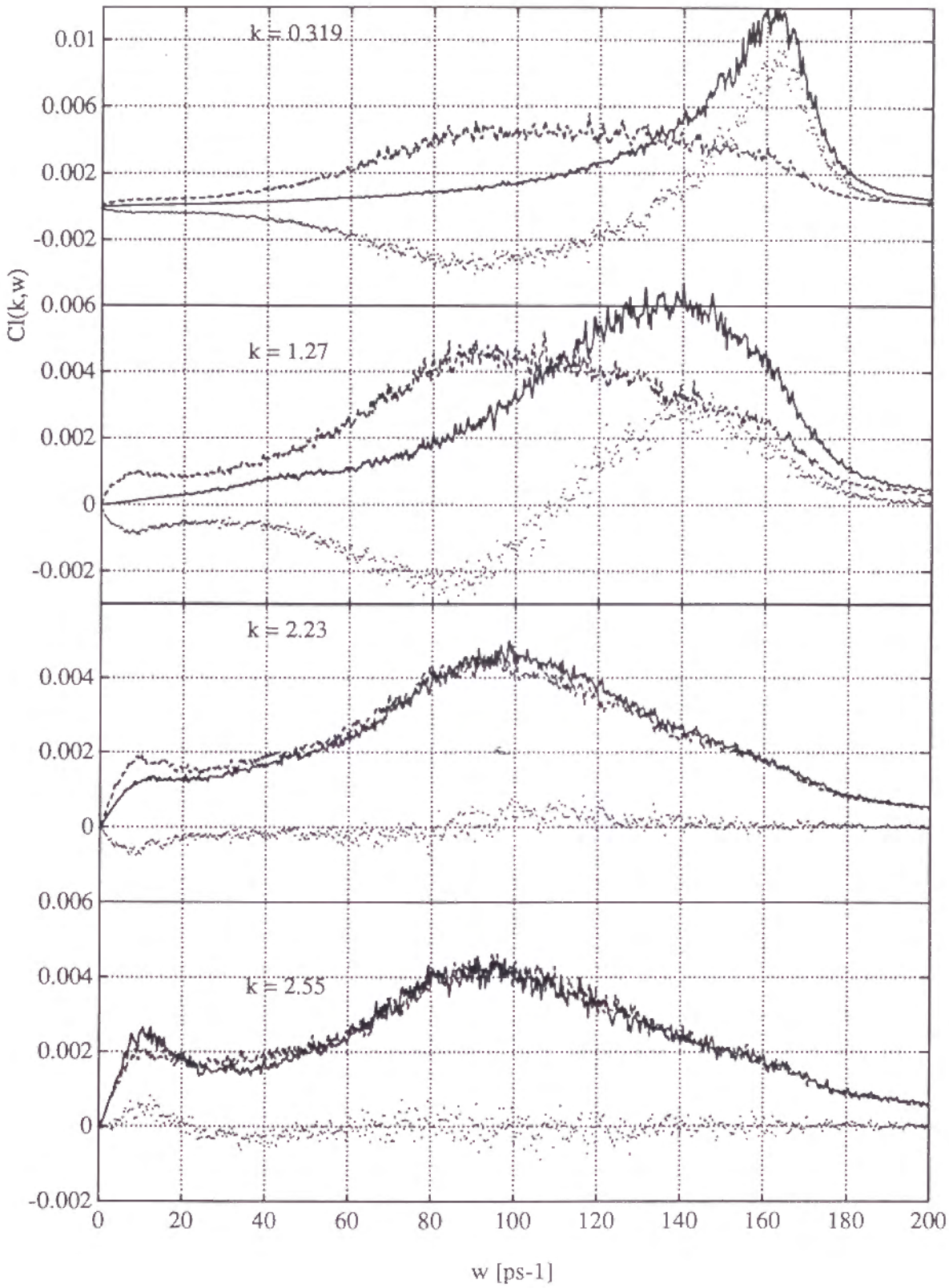
k = 0.319
k = 1.27
k = 2.23
k = 2.55
Cl(k,w)
w [ps-1]
0.01
0.006
0.002
-0.002
0.004
0
20
40
60
80
100
120
140
160
180
200

Fig. 8

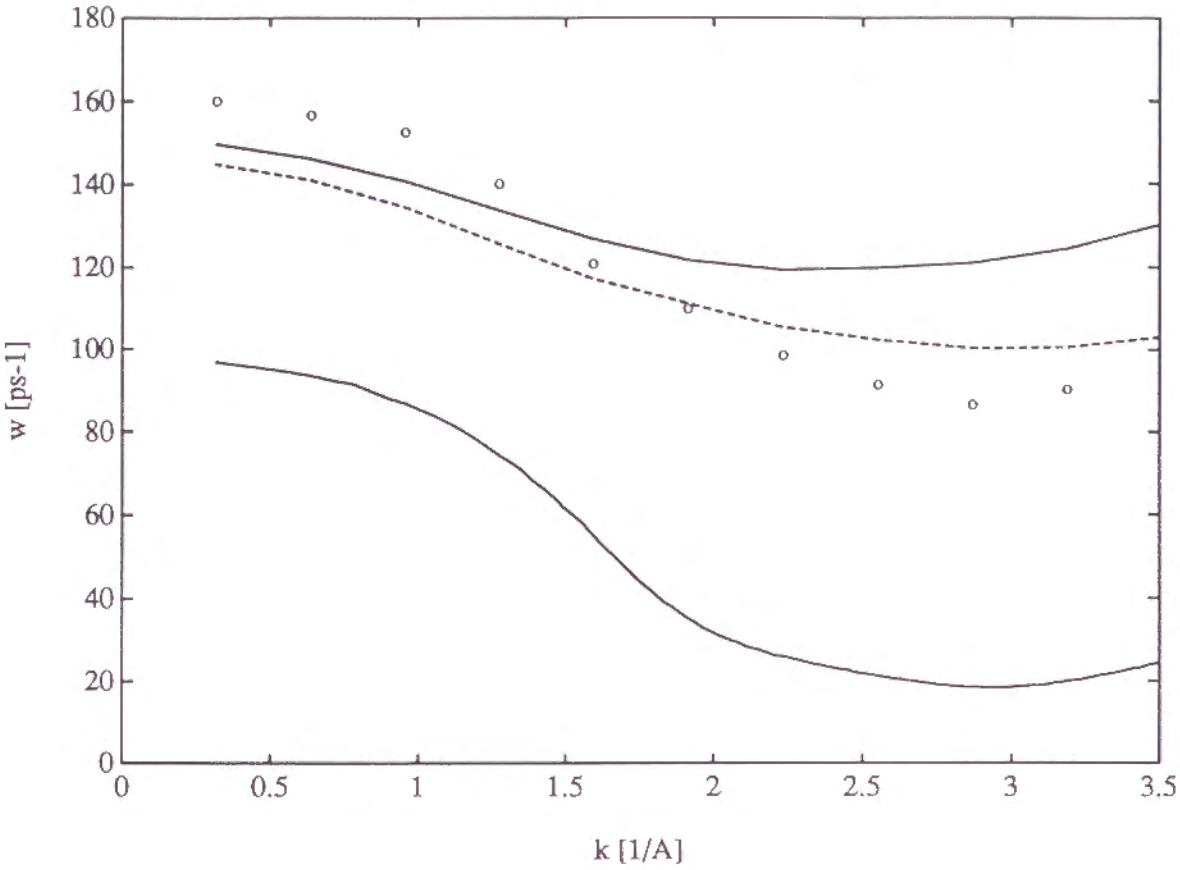

Fig. 9

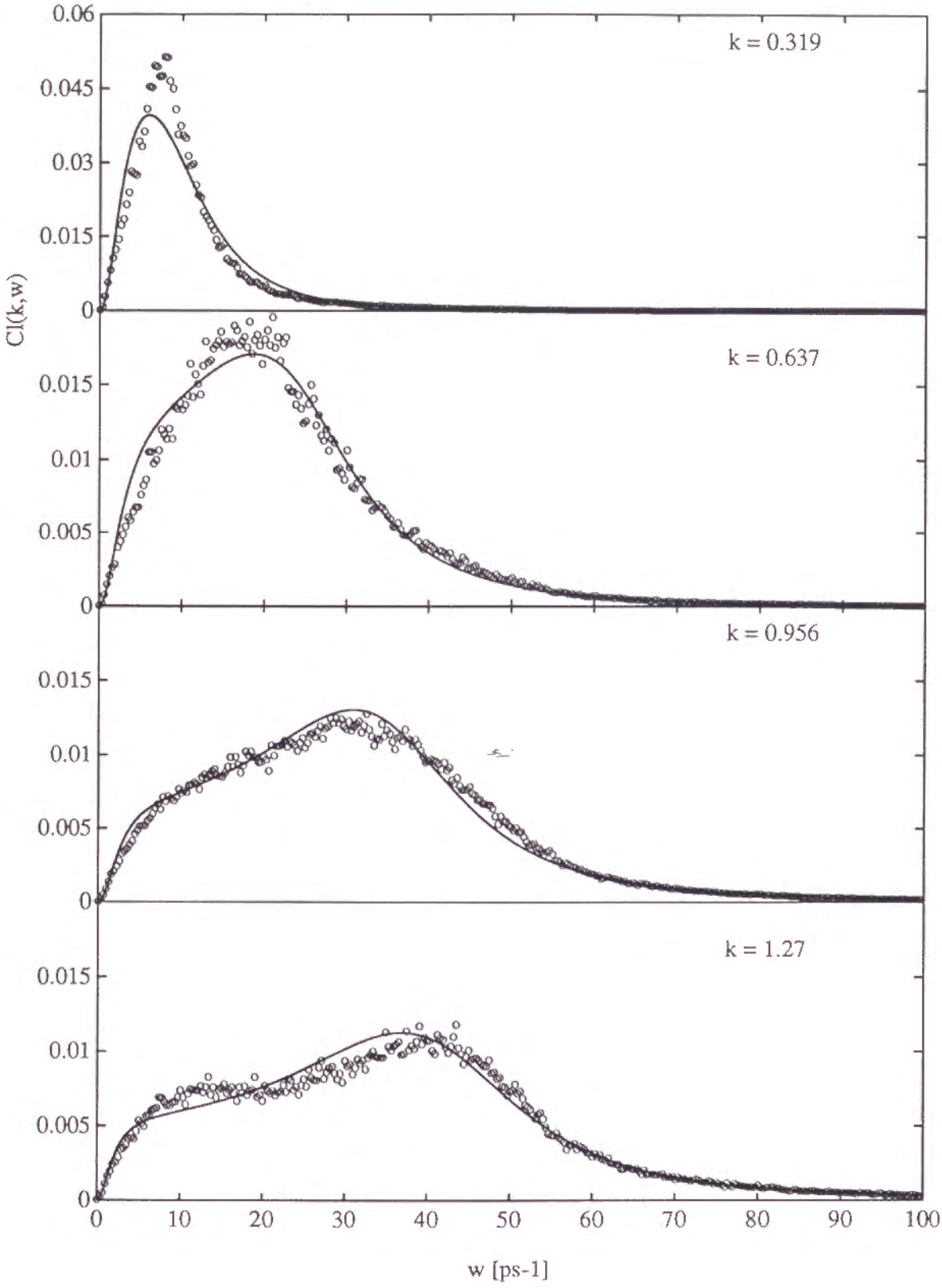
k = 0.319
k = 0.637
k = 0.956
k = 1.27
Cl(k,w)
w [ps-1]
0.06
0.045
0.03
0.015
0
0.01
0.005
10
20
30
40
50
60
70
80
90
100

Fig. 10

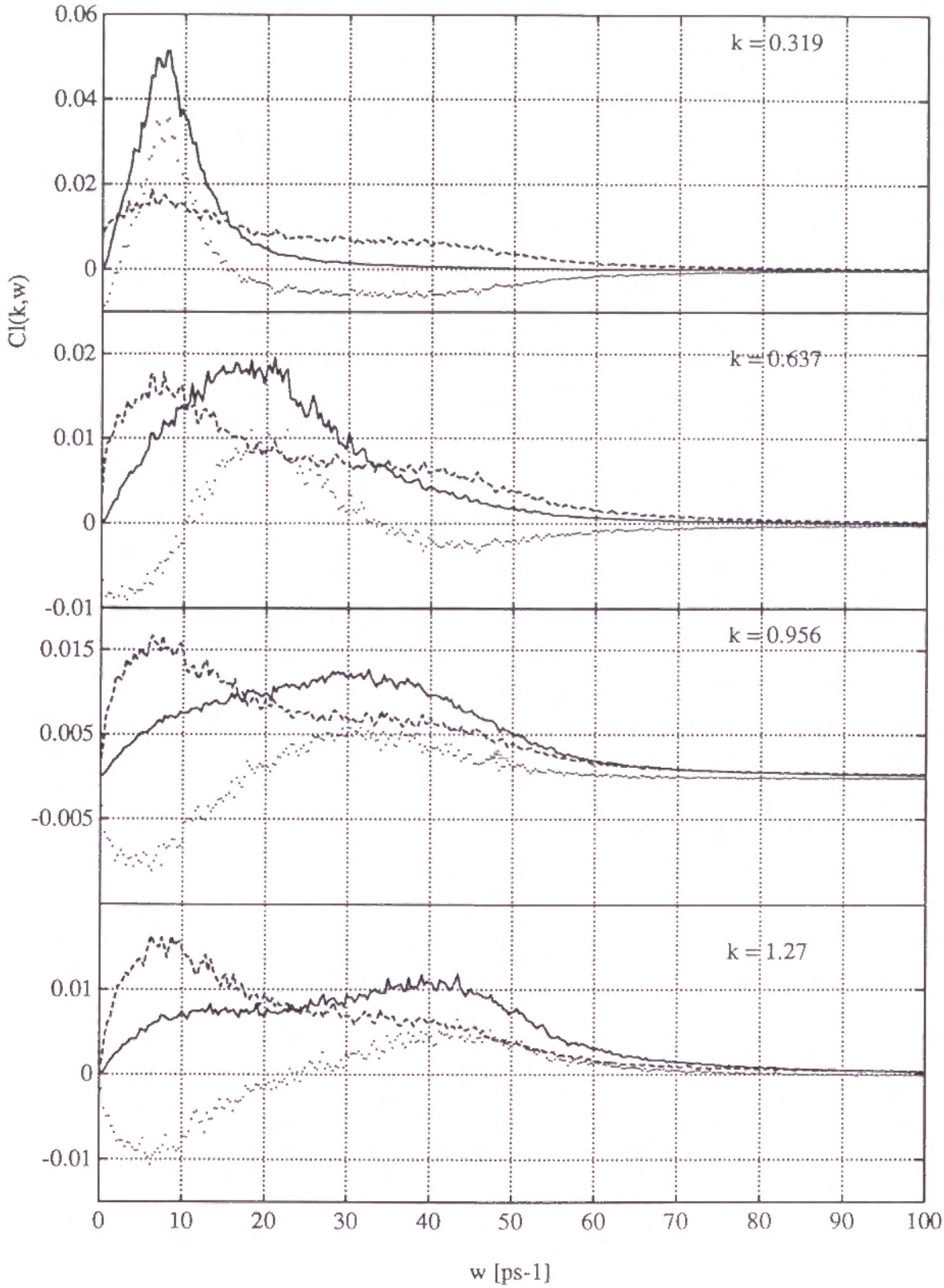
k = 0.319
k = 0.637
k = 0.956
k = 1.27
Cl(k,w)
w [ps-1]
0.06
0.04
0.02
0
0.02
0.01
0
-0.01
0.015
0.005
-0.005
0.01
0
-0.01
0
10
20
30
40
50
60
70
80
90
100

Fig. 11

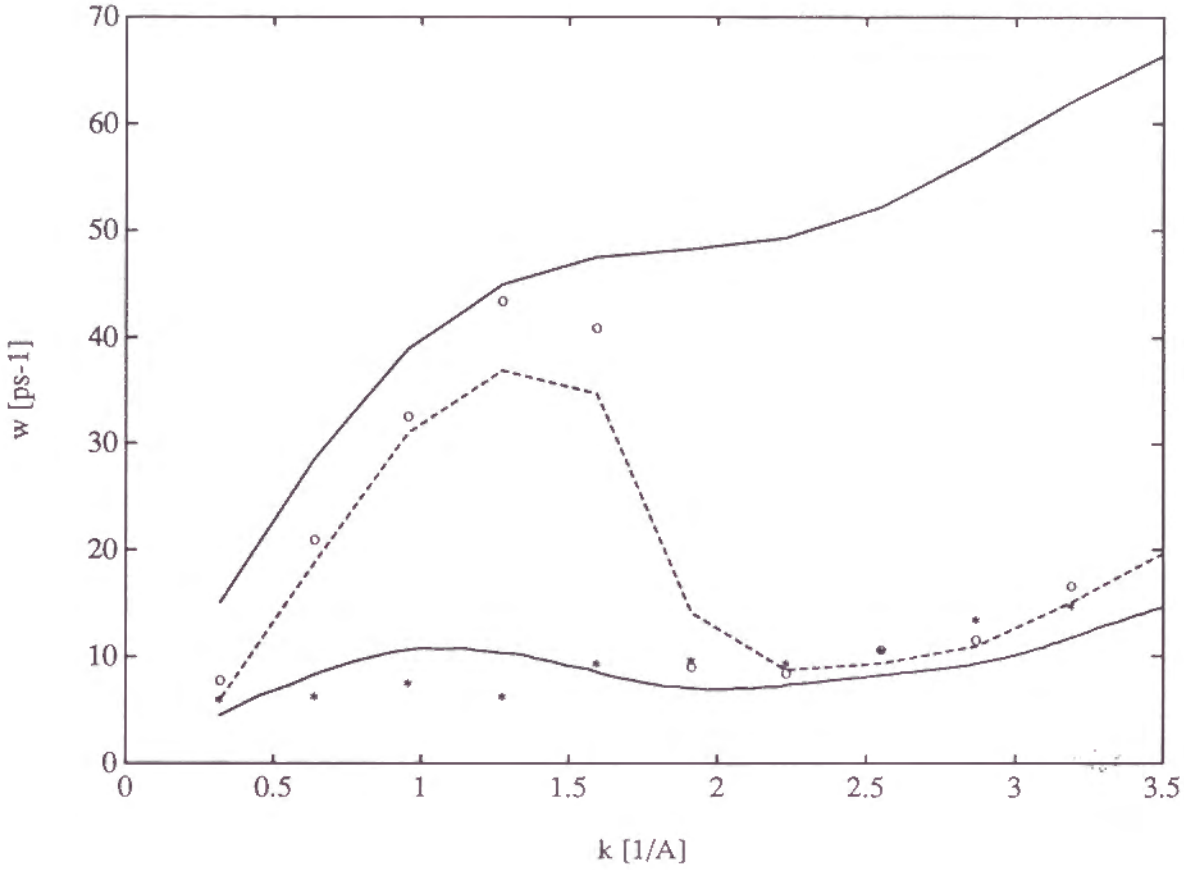

Fig. 12

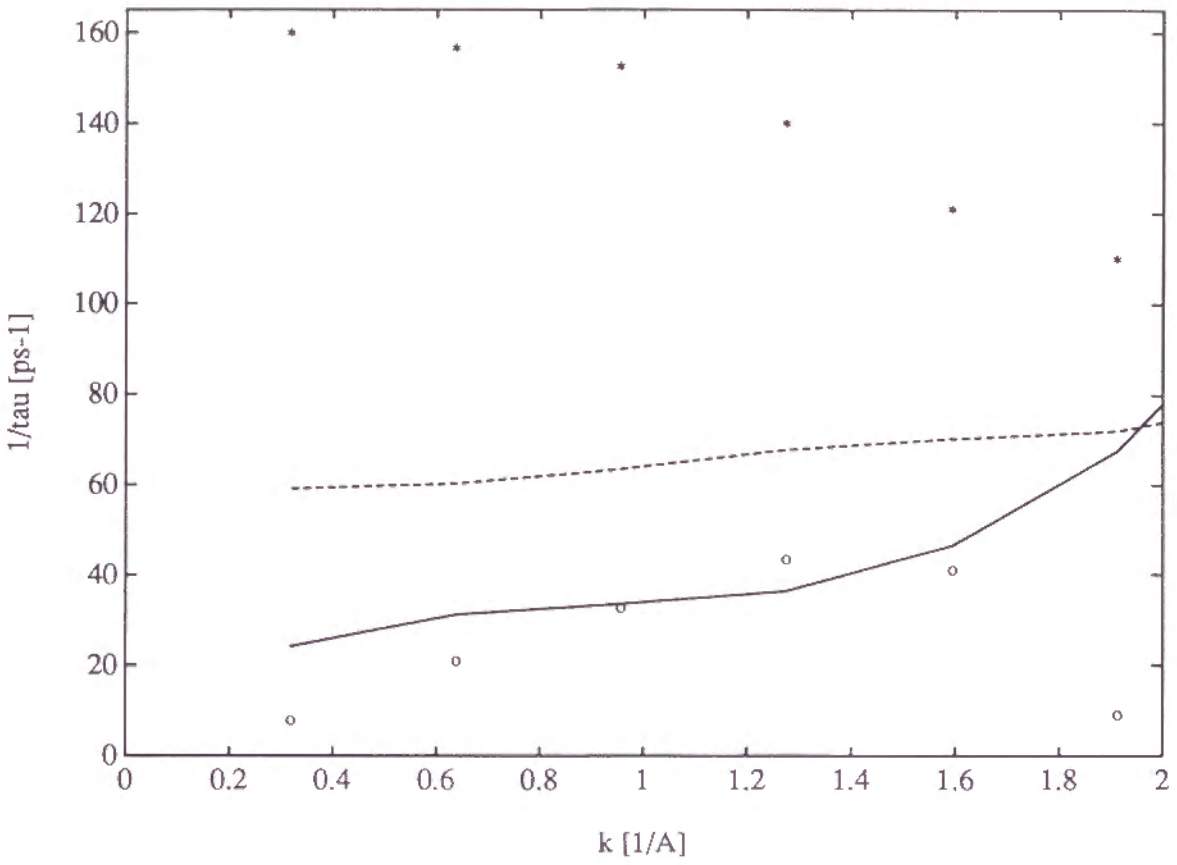
160
140
120
100
80
60
40
20
0
1/tau [ps-1]
0
0.2
0.4
0.6
0.8
1
1.2
1.4
1.6
1.8
2
k [1/A]

Fig. 13

IV. Conclusions and problems for future study

The stability of the hydrated electron and the collective excitations in liquid water have been studied theoretically. In chaper II, the integral equation theory for the solvated electron, the RISM-polaron theory, has been applied to the problem of the excess electron in water. We have paid special attention to the temperature dependence of the stability of the hydrated electron. The detailed study presented in chapter II has led us to the following conclusions:

(i) The average potential energy and the cavity formation energy of the excess electron have a minimum and a maximum, respectively, as temperature increases. The extrema are manifestation of balance between two opposing process caused by the disruption of the hydrogen bonds between water molecules. Essentially the same cause makes extrema in the temperature dependence of thermodynamic quantities of water including the compressibility for which theoretical calculation has been also demonstrated in the present work.

(ii) The excess chemical potential of the hydrated electron predicted by the theory is in good agreement with experiment. The excess electron stabilizes with increasing temperature. This is opposite temperature dependence in comparison with classical anion as Cl^-. The classical part of excess chemical potential which is obtained by subtracting the kinetic energy from the chemical potential shows the same tendency as Cl^-. Consequently, temperature dependence is determined by that of the average kinetic energy of the excess electron.

(iii) The binding energy, which is a sum of the average kinetic energy and the potential energy, also exhibits a minimum around 60 °C. It is suggested to measure

the quantity to probe the anomalous temperature dependence in thermodynamic quantities of the hydrated electrons.

(iv) The first excitation energy of the excess electron was estimated from the mean square displacement of the electron in imaginary time. Absolute values were overestimated, however, temperature dependence was in very good agreement with experiment. The observed red shift of the peak of the optical absorption spectrum with increasing temperature was successfully reproduced. This gives us confidence on our results from the RISM-polaron theory.

Our calculations are based on two integral equation theory, one is the extended RISM theory to calculate the structure factor of pure water and the other is the RISM-polaron theory to calculate the dispersion of the excess electron and the correlation between the electron and water molecules. In contrast with our calculations, Laria *et al.*[1] estimated the structure factor from the molecular dynamics simulation of pure water. However, it is not convenient for the MD simulation to calculate the thermodynamic quantities such as isothermal compressibility, which play important roles in discussing the stability of a hydrated electron. One advantage of the extended RISM theory is that it is easy to calculate those thermodynamic quantities with qualitatively reasonable accuracy from the pair correlation functions. It can be concluded that the integral equation approach gives a reasonable and convenient route to discuss the microscopic behavior of the excess electron in polar liquid.

In chapter III, the collecitve and single molecule excitations concerning mass and charge fluctuation has been investigated theoretically and by the MD simulation. The detailed analysis had led us to the following conclusion:

(i) The mass and charge densities represented by fluctuating site densities are introduced to describe the acoustic and optical behavior in liquid water. The eigen frequencies of mass and charge fluctuations are determined by the projection operator formalism. These two eigen frequencies give the correct long wavelength limit expected from the acoustic and optical behavior of the system.

(ii) Our non-damping theory predicts the amplitudes of mass and charge modes in density correlation functions. The charge mode gives little influence on the dynamics of mass fluctuation, whereas the mass mode changes the dynamics of charge fluctuation considerably with increasing k. Our theory shows that the amplitude of mass mode in $F_{ZZ}(k,t)$ grows rapidly above the wavevector 1.0 Å^{-1}. This is caused by the coupling of translational mode to the charge fluctuation through the single molecule correlation, which gives the slow tail in $F_{ZZ}(k,t)$.

(iii) The anomalous acoustic behavior in liquid water is examined. The high sound velocity at $k < 1.5$ Å^{-1} is observed, however, there exists only one peak in $C^{L}_{MM}(k,\omega)$ at each k simultaneously. The low frequency structure of the mass current spectrum above the wavevector 1.0 Å^{-1} can be attributed to the single molecule excitation, not the collective one as sound wave. The mass current spectrum and the dispersion relation are analyzed by the simple viscoelastic theory. A good fit of the spectrum is achieved and the anomalous behavior of the acoustic branch is well reproduced. Consequently, we can conclude that the high sound velocity is a result of the continuous positive dispersion of the normal sound. The anomaly concerning the acoustic behavior lies in the unexpectedly high value of the phonon frequency of the acoustic mode.

(iv) The dynamics of charge fluctuation is well characterized by the phonon

frequency of the optical mode, $\omega_{LO}(k)$ at k < 1.5 Å^{-1}. The frequency $\omega_{LO}(k)$ is also much larger than $\omega'_0(k)$ because of the strong short-rang interaction between water molecules. Our phenomenological model of charge current spectrum reproduces the simulation results qualitatively. The small shear relaxation rate in comparison with $\omega_{LO}(k)$ leads the oscillatory behavior of charge fluctuation nearly by $\omega_{LO}(k)$.

At the wavevector k <1.5 Å^{-1}, the charge fluctuation shows "elastic" dynamics characterized by the phonon frequencies in the time scale of the inverse of $\omega_{CZ}(k)$. A normal mode analysis of liquid water[2] may give a good guide to describe the dynamic structure factor of charge density. On the other hand, the mass fluctuation shows "viscoelastic" behavior, which means that the fluctuation decays after one or two oscillations. This suggests that the period of oscillation ≈ a few sub-picoseconds is close to the residence time of the system in a minimum of the configuration space. It has been shown that the transition of the system between basins in the configuration space occurs once in sub-picoseconds.[2] To understand this problem profoundly, the relation between the "viscoelastic" behavior and the intra and inter basin dynamics of the system should be examined.

To give a final answer to the anomalous acoustic behavior of liquid water, we have to construct a molecular theory covering from long to small wavelength on a unified basis. A mode coupling theory is promising,[3] however, the explicit expressions of phonon frequencies for ISM liquid should be derived first. These are future problems.

References

[1] D. Laria, D. Wu and D. Chandler, J. Chem. Phys. **95**, 4444 (1991).

[2] I. Ohmine and H. Tanaka, Chem. Rev. **93**, 2545 (1993).

[3] J. Bosse, W. Götze and M. Lücke, Phys. Rev. A **17**, 434 (1978); J. Bosse and T. Munakata, Phys. Rev. A **25**, 2763 (1982).